Investigation of rotating spoke instabilities in a wall-less Hall thruster. Part I: Experiments.

IEPC-2017-248

Presented at the 35th International Electric Propulsion Conference
Georgia Institute of Technology – Atlanta, Georgia – USA
October 8–12, 2017

S. Mazouffre*, L. Grimaud† and S. Tsikata‡
CNRS, ICARE, EP team, 1c avenue de la recherche scientifique, 45071 Orléans, France.

K. Matyash§ and R. Schneider¶
Ernst-Moritz-Arndt University, Greifswald, D-17487, Germany.

Properties of rotating spokes have been investigated in the low-pressure low-temperature plasma discharge of the 200 W-class permanent magnet ISCT200 Hall thruster in wall-less configuration. For comparison purposes, the Hall thruster was also operated in the standard configuration. High-speed camera imaging combined with sophisticated image processing allowed to observe the plasma inhomogeneity dynamics and to determine characteristics such as mode number, sizes, rotation frequency and propagation velocity. The time varying Xe^+ ion velocity distribution function has been measured in front of the anode of the ISCT200-WL thruster by means of photon counting LIF spectroscopy. Numerical simulations have been performed in parallel with a 3D-3V PIC code. Several similarities have been found between experiments and simulations. The time-dependent ion VDF in the azimuthal direction could be reconstructed from the numerical data set, which confirmed the existence of ions with positive and negative velocities within the plasma structure.

Nomenclature

A	Surface area	m^2	m	Mode number	–
$\mathbf{B}$	Magnetic field	G	n	Density	m^{-3}
c_s	Ion acoustic speed	m/s	p	Pression	Pa
d	Channel diameter	m	r	Radius	m
$\mathbf{E}$	Electric field	$\mathrm{V\,m^{-1}}$	t	Time	s
f	Frequency	Hz	T	Period; Temperature	s, K
ϕ	Potential	V	θ	Angle	rad, °
Φ	Mass flow rate	$\mathrm{kg\,s^{-1}}$	U_d	Applied voltage	V
h	Channel width	m	v	Velocity	$\mathrm{m\,s^{-1}}$
I_d	Discharge current	A	ω	Angular velocity	rad/s
λ	Wavelength	m	x, y, z	Coordinates	m

*Director of Research, Head of electric propulsion team, ICARE, stephane.mazouffre@cnrs-orleans.fr
†PhD student, ICARE, lou.grimaud@cnrs-orleans.fr
‡Research scientist, ICARE, sedina.tsikata@cnrs-orleans.fr
§Research scientist, Head of HPC group, Greifswald University, knm@ipp.mpg.de
¶Professor, Greifswald University, Head of Computer Center, schneider@uni-greifswald.de

I. Introduction

Rotating plasma inhomogeneities, often termed "rotating spokes", are observed in various types of magnetized low pressure plasma discharges created in a crossed electric and magnetic field configuration.[1–4] Over the past ten years, such structures have been experimentally investigated e.g. in plasma devices like magnetrons[5–10] and Hall thrusters.[11–17] There is a great deal of interest in studying rotating plasma structures for mainly two reasons. Firstly, such instabilities seem to be a very general phenomenon in low-pressure low-temperature partially magnetized plasma discharges of which the origin and the governing mechanisms are not yet fully understood. Secondly, these large-scale low-frequency rotating instabilities certainly play a role in the transport of charged particle across the magnetic field lines. As a consequence, rotating spokes probably influence characteristics and performances of plasma devices and plasma technologies like thin-film deposition and spacecraft propulsion.

In this contribution we experimentally examine the properties of low-frequency rotating plasma instabilities in the discharge of the low power ISCT200 Hall thruster. The ISCT200 – an acronym for ICARE Small Customizable Thruster – is a versatile 200 W-class Hall thruster using permanent magnets for generating the magnetic field instead of helical magnetizing coils.[18,19] Two different configurations of the ISCT200 thruster have been employed for the study: the standard (ST) one and the wall-less (WL) one. The main objective of this work was to characterize the physics and the dynamics of rotating plasma structures in the $E \times B$ discharge of a 200 W-class Hall thruster by means of two diagnostic techniques. High-speed camera imaging has been used to capture the rotating spoke motion and transformation for various thruster operating conditions. Image processing with sophisticated algorithms allowed to determine the rotation velocity, direction and frequency, the plasma structure shape and sizes and the mode number. Time-resolved Laser-Induced Fluorescence spectroscopy in the near infrared has been employed to record the temporal evolution of the ion azimuthal velocity component during the rotation of a plasma inhomogeneity. Here, a novel photon counting approach has been developed to enable measurements without externally stabilizing the discharge.

The deep analysis of data acquired for the two Hall thruster configurations by means of fast camera imaging and laser spectroscopy allows us to present and to discuss the following points:

- properties of rotating spokes in terms of velocity, frequency, domain of existence and correlation with longitudinal instabilities such as breathing oscillations,
- impact of the discharge voltage, propellant mass flow rate and cathode heater current on the properties of the rotating inhomogeneities,
- time evolution of the ion VDF in the course of a spoke rotation,
- comparison of the features of rotating structures in conventional and wall-less Hall thrusters.

Notice the numerical investigation of rotating spokes in the discharge of our 200 W Hall thruster in wall-less configuration will be presented in a companion paper, see IEPC paper 2017-403. Some comparisons between experimental results and numerical outcomes are, however, included in this article.

II. Experimental apparatus

A. 200 W Hall thrusters

The Hall thruster used in this work about the physics of rotating plasma structures is the ISCT200 thruster. ISCT is an acronym for ICARE Small Customizable Thruster. The ISCT200 is a versatile 200 W-class Hall thruster using permanent magnets for generating the magnetic field instead of helical magnetizing coils.[18,19] Two different configurations of the ISCT200 have been employed: the standard (ST) one and the wall-less (WL) one. The two versions, however, share many common features, namely:

- The annular channel mean diameter is around 40 mm.
- The channel geometry is in the so-called $2S_0$ configuration, that means the channel width-to-mean diameter ratio h/d is twice the standard one, where this standard ratio is defined as that of the well-known Russian SPT100 thruster. As demonstrated in a preceeding study, a broad channel improves the performance level of a Hall thruster in terms of thrust, mass utilization, ion production cost, ion velocity, thermal load, and operation envelope.[18]

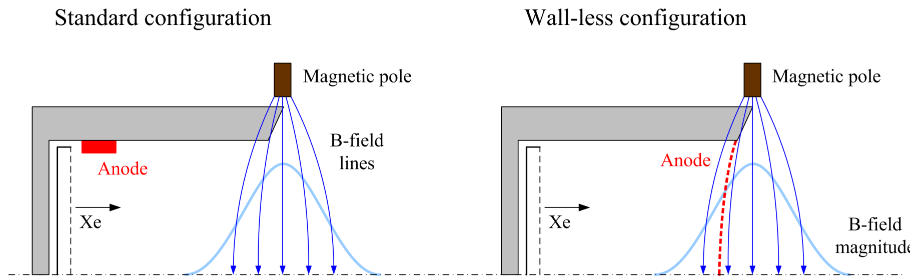

Figure 1. Schematic of anode layout and magnetic field topology for the standard (left) and Wall-Less (right) configurations.

- The inner and outer channel walls are made of BN-SiO_2 ceramic.
- A set of small SmCo permanent magnets combined with a soft iron magnetic circuit generate the magnetic field. No magnetic screen is used. The magnetic field topology stays unchanged for the two configurations with magnetic field lines perpendicular to the channel walls at the channel outlet. The magnetic field is directed inwards, consequenctly the $E \times B$ electron drift propagates clockwise.
- The magnetic field strength is the highest on the channel axis at the channel exit plane: $B_{\max} \approx 300\,\mathrm{G}$.
- A porous mullite ceramic placed at the back of the channel serves as gas injector.
- Heat pipes made of copper evacuate the heat towards a large radiator installed at the back of the thruster body.
- The thruster body is floating.

A heated hollow cathode with a disk-shaped LaB_6 emmiter was used with the two versions.[20] The cathode, which produces the electron current for discharge balance and ion beam neutralization, is located outside the channel. The cathode is electrically connected to the thruster anode and floating. High-purity Xenon (Xe) was used as the propellant gas for both the thruster discharge and the cathode discharge. The cathode has been operated with a constant Xe mass flow rate of 0.2 mg/s, below its normal operating conditions (0.4 mg/s). Typically, about 150 W electrical power is applied to the cathode to sufficiently heat-up the emitting element.

1. *Standard configuration*

The main differences between the two ISCT200 thruster configurations are in fact the anode geometry and location. In this version, the anode is a 5 mm in height and 1 mm in thickness stainless steel ring placed at the back of the channel against the internal surface of the outer dielectric wall.[18]

2. *Wall-less configuration*

The wall-less configuration is a recent and original approach to decrease plasma-wall interactions, hence prolonging the thruster lifetime.[21,22] A well-established approach to reduce ion bombardment in the final sectio of the channel wall of a HT is termed magnetic shielding (MS).[23–31] It consists of preventing the magnetic field lines from crossing the walls in the acceleration region. The MS field topology is formed by these parallel lines near the walls, also termed grazing lines, which extend to the anode region where electrons are cold. This in turn allows the maintenance of a high plasma potential in front of the walls. Such a topology strongly reduces the magnitude of the radial electric field component, thereby decreasing ion energy and the wall material erosion rate without decreasing the performance.

There is another more drastic alternative to limiting the interaction between plasma and surfaces in a HT. The principle is to entirely shift the ionization and acceleration regions outside the cavity. This unconventional design is named a Wall-Less Hall Thruster, or WL-HT in short.[21,22,32] Such an unusual configuration was in fact first explored during the 90s in Russia by Kapulkin et al.[33,34] To shift both the ionization and the acceleration regions outside the thruster cavity, the anode is moved towards the channel

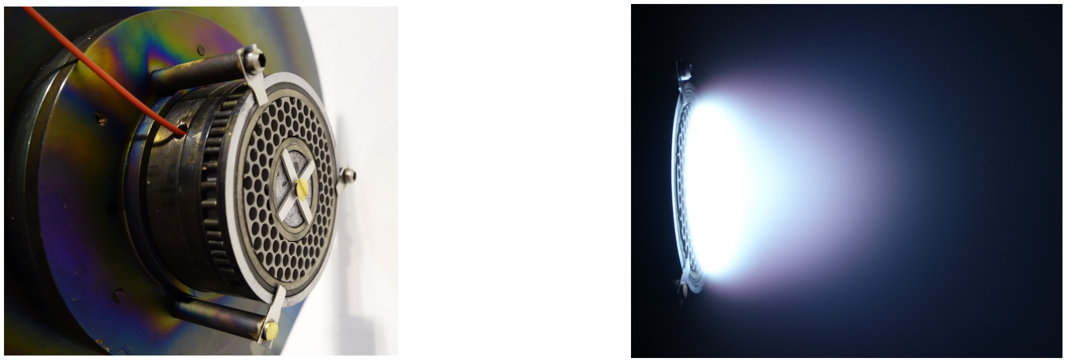

Figure 2. Picture of the ISCT200 Hall thruster in WL configuration with a gridded anode at the channel exit plane (left) and photograph of the thruster firing with Xe in the NExET test-bench.

exit plane without other modifications. The thruster shape and size remain unchanged, as do the cavity material and the magnetic field topology. Notice a Wall-Less Hall thruster is not a Thruster with Anode Layer,[35] as there is no guard ring at the cathode potential in front of the anode to localize the potential drop.

Figure 1 illustrates the anode architecture and the magnetic field topology in the basic configuration and in the WL configuration as well. The magnetic circuit of the ISCT200 thruster used in this study was based on that of a classical Hall thruster. Therefore, the B-field lines are perpendicular to the thruster axis. In standard configuration, the anode is located at the back of the channel, far from the magnetic barrier. In WL mode, the anode is placed at the channel exhaust. To warrant an efficient confinement of electrons downstream the channel exit plane, therefore keeping performances to a good level, the magnetic field lines must not intercept the anode at all.[22] A possible solution is to use a gridded anode with a curved surface in such a way the anode surface is parallel to the magnetic field lines.[36] Here the anode is a 1 mm tick grid with 3 mm in diameter circular holes. The anode transparency is 0.68, which allows a homogeneous propellant gas distribution outside the channel. A photograph of the ISCT200 Hall thruster in WL configuration with its curved gridded anode at the channel exit plane is displayed in Fig.2. The same figure shows the ISCT200-WL thruster firing with Xe at 1 mg/s and 200 V discharge voltage in the NExET vacuum chamber. As can be seen, the plasma discharge is detached from the anode, the signature for an efficient confinement.

From a technological point of view, a wall-less configuration may be a promising approach to offer a low-cost compact thruster with a long life span and able to operate at large discharge voltages, that means at large specific impulses. Moreover, due to a very large surface-to-volume ratio, a WL-type configuration is probably easier to scale up to large input power and down to very low power compared for instance to a classical Hall thruster architecture.

From a more fundamental perpsective, a wall-less ion source provides an ideal platform for the study of cross-field discharge configurations with electrostatic probes and with sophisticated tools like coherent and incoherent Thomson scattering and Laser Induced Fluorescence spectroscopy. The access it provides to key regions of the plasma facilitates a thorough investigation of plasma instabilities and small scale turbulence for a better understanding of the discharge physics and anomalous electron transport. Additionally, it allows to study these phenomena without the influence of wall processes such as secondary electron emission and sputtering. A WL Hall thruster is also an adequate configuration to make comparisons between experiments and computer simulations. Due to a simplified architecture, boundary conditions are easier to model, which permits to obtain more accurate and more reliable numerical outcomes. For all aforementioned reasons, the Wall-Less configuration has been selected to investigate the physics of rotating plasma inhomogeneities in the discharge of the Hall thruster.

B. NExET vacuum chamber

All experiments that involved the ISCT200 Hall thruster have been performed in the cryogenically-pumped NExET (New Experiments on Electric Thrusters) vacuum chamber. NExET is based on a 1.8 m in length and 0.8 m in diameter stainless steel tank. Primary pumping is ensured by a dry pump that evacuates 400 m^3/h. A 350 l/s turbomolecular pump is capable of further evacuating the chamber down to 10^{-6} mbar-N_2,

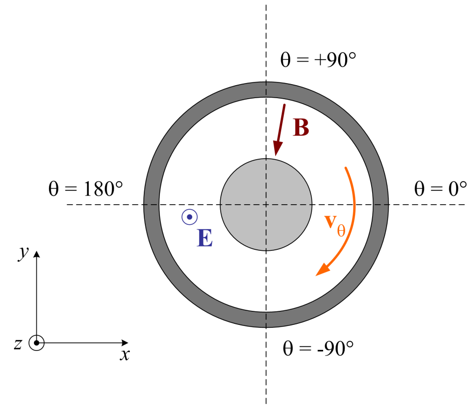

Figure 3. Front view diagram of a HT with the reference system for angles and spatial coordinates. Also shown are the E and B vectors and the drift velocity. Directions correspond to the ones of the ISCT200 thrusters.

by absorbing light gases such as N_2, O_2, H_2O and H_2. The cryogenic pump absorbs gases such as xenon and krypton. The pumping speed is around 8,000 l/s when the $0.5\,\mathrm{m}^2$ cold panel is sustained at 35 K. The overall pump stack warrants a background pressure as low as 2×10^{-5} mbar-Xe during operation of a 400 W input power plasma source. The heavy particle momentum exchange mean free path is, in this backpressure condition, on the order of the chamber length, which guarantees a negligible impact of the residual gas on the source operation and measurement outcomes. A large water-cooled screen covered with graphite tiles is mounted at the back of the chamber. It absorbs a part of the ion beam energy, therefore reducing the thermal load onto the cryogenic surface. The chamber is equipped with several observation windows, access ports and vacuum feed-through connectors for power lines, gas lines and diagnostic tools. A large front door enables easy access to the interior of the vessel.

C. Coordinate system

Figure 3 indicates the reference system for angles and Cartesian coordinates used in this study. Angles are defined according to the unit circle.

Also shown in Fig. 3 are the electric field and magnetic field vectors as well as the associated $E \times B$ electron drift velocity. Electrons rotates clockwise in the figure that corresponds to the ISCT200 Hall thruster configuration used in this work.

III. Diagnostic techniques

A. LIF spectroscopy

1. Optical bench

The time-averaged time-varying distribution functions of the velocity components of the Xe^+ ion have been measured by means of Laser-Induced Fluorescence (LIF) spectroscopy in this study. The LIF technique has been extensively described elsewhere, see[37,38] and references herein. Only a brief description of the LIF optical train is given here.

An amplified tunable single-mode external cavity laser diode is used to excite metatstable Xe^+ ion at 834.72 nm. The laser wavelength is accurately measured by means of a calibrated wavemeter. A scanning confocal Fabry–Perot interferometer is used to real-time check the quality of the laser mode and to detect mode hops. The power of the beam is also continuously monitored. The primary laser beam is modulated by a mechanical chopper at a frequency around 2 kHz to allow phase sensitive detection of the fluorescence signal. The laser beam is coupled into a single-mode optical fiber and carried into the NExET vacuum chamber. At the exit of the optical fiber, collimation optics form a 1 mm in diameter beam of which the power is maintained below $5\,\mathrm{mW/mm}^2$ to avoid a strong saturation of the optical transition. The fluorescence radiation at 541.91 nm is collected using a 40 mm focal length lens that focuses the light onto a 200 μm core

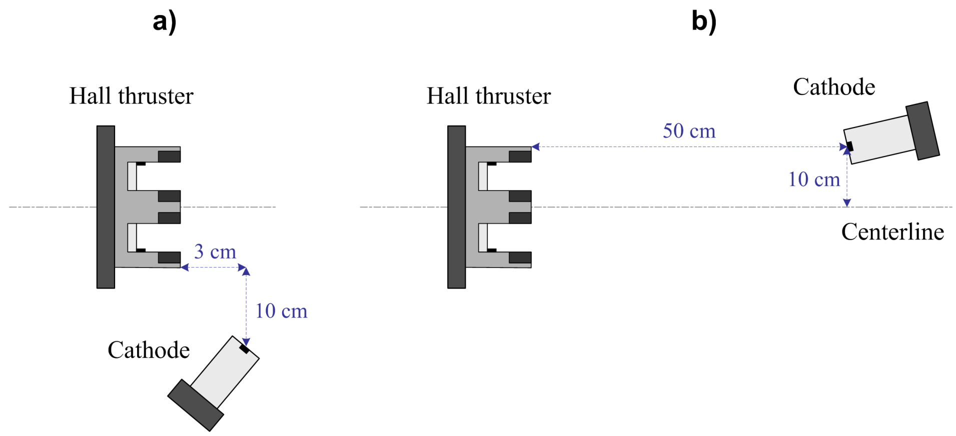

Figure 4. Schematic showing the two cathode locations tested with the ISCT200-WL thruster (not to scale): Case (a) down position and case (b) ∼ on-axis position.

diameter multimode fiber. The magnification ratio is 1:1. The fluorescent light transported by the fiber is focused onto the entrance slit of a 20 cm focal length monochromator that isolates the fluorescence line from the rest of the spectrum. A photomultiplier tube serves as a light detector. In time-averaged mode, a lock-in amplifier operating at the chopper frequency is used to discriminate the fluorescence light from the intrinsic plasma emission.

2. Impact of the cathode location

The external cathode location can influence the ion trajectory and velocity vector, as demonstrated in a previous study.[39] Experiments performed by means of LIF spectroscopy at 834.72 nm on metastable Xe^+ ions in the near-field plume of a 1.5 kW-class SPT100 Hall thruster revealed the ion azimuthal velocity components is perturbed by the cathode. The ion azimuthal velocity is not only driven by the magnetic deflection but a weak transverse electric field directed toward the external cathode must be accounted for. This electrid field certainly originates from the fact that the cathode potential is below the downstream plasma potential. The cylindrical symmetry of the discharge therefore breaks and the thrust vector is slightly tilted, which induces a small torque in the Hall thruster.[39]

Before starting the study on rotating plasma structures in the discharge of the ISCT200 thruster, it was relevant to investigate a possible influence of the cathode placement on the ion azimuthal velocity. As can be seen in Fig. 4, two cathode positions have been tested: below the thruster main body and far away in the plasma plume.

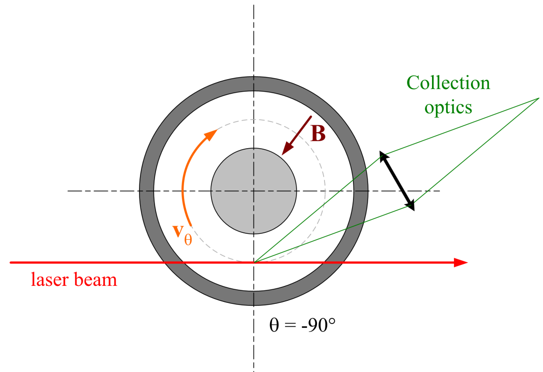

Figure 5. Front view diagram of the ISCT200 thruster with the laser beam and fluorescence light collection optics for the LIF experiments. The B field and drift velocity vectors are also given.

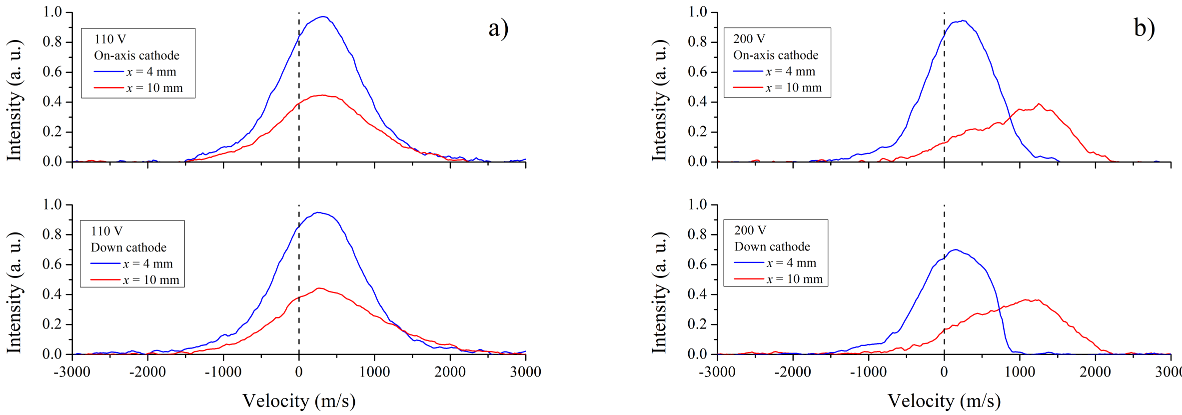

Figure 6. Distribution of the Xe^+ ion azimuthal velocity for the two cathode positions. $v > 0$ in the $E \times B$ drift direction. a) $U_d = 110\,\mathbf{V}$ and $\Phi_a = 1.2\,\mathbf{mg/s}$. b) $U_d = 200\,\mathbf{V}$ and $\Phi_a = 0.8\,\mathbf{mg/s}$

3. Ion velocity in the azimuthal direction

Measurements have been performed with the ISCT200-WL thruster behind the channel exit plane. The measurement locations were located on the channel axis at $x = 4\,\mathrm{mm}$ and $x = 10\,\mathrm{mm}$ and $\theta = -90°$, as illustrated in Fig. 5. The axial position were selected to enable measurements in the ionization region ($x = 4\,\mathrm{mm}$) and in the acceleration layer ($x = 10\,\mathrm{mm}$).[21]

Figure 6a shows the Xe^+ ion azimuthal velocity distribution function (VDF) measured at 110 V applied voltage, 1.2 mg/s mass flow rate and 0.94 A discharge current for the two cathode positions. A positive velocity indicates ion rotate in the $E \times B$ electron drift direction by convention. As can be seen in Fig.6a, neither the cathode position, nor the measurement axial position influence the ion VDF. The magnitude of the most probable Xe^+ ion azimuthal velocity is given in Tab.1 for all cases.

Figure 6b shows the Xe^+ ion azimuthal VDF measured at 200 V applied voltage, 0.8 mg/s mass flow rate and 0.69 A discharge current for the two cathode positions. As can be seen in Fig.6b the cathode position has no impact on the ion VDF. On the contrary, the measurement position influences the ion velocity. As will be shown in section V and VI, there is no well-defined rotating plasma structure at 200 V ($m = 0$ mode) whereas a rotating structure is present at 110 V ($m = 1$ mode). Another difference is the magnitude of the axial electric field component, which is larger at 200 V. The discrepancy observed in Fig. 6b can have two origins. Firstly, a slight misalignement of the laser beam in the horizontal plane can drastically change the measured Doppler shift. The latter being given by the $\mathbf{k}\cdot\mathbf{v}$ product, where $\mathbf{v}$ is the ion velocity vector, a misalignement adds the v_z component which is large. Secondly, the ion azimuthal velocity magnitude depends on the distance travelled by ions in the cross-field region, see.[39] A larger ion velocity is therefore expected at $x = 10\,\mathrm{mm}$. The magnitude of the Xe^+ ion azimuthal velocity is summarized in Tab.1.

For the remainder of the study, the cathode was located in the far-field plume region above the thruster centerline, i.e. case (b) in Fig. 4.

Table 1. Most probable Xe^+ ion azimuthal velocity for the two cathode positions.

Cathode	Axial position	
	5 mm	10 mm
$U_d = 110\,\mathrm{V}$		
On-axis	312 m/s	326 m/s
Down	282 m/s	289 m/s
$U_d = 200\,\mathrm{V}$		
On-axis	227 m/s	1249 m/s
Down	165 m/s	1154 m/s

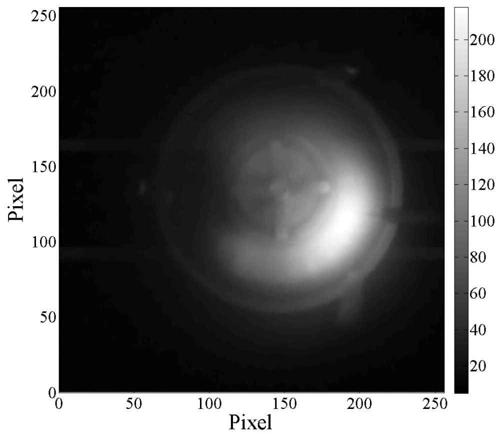

Figure 7. Snapshot of the rotating plasma structure in the discharge of the ISCT200-WL thruster operating at 110 V. Filtered image with a 8-bit grayscale.

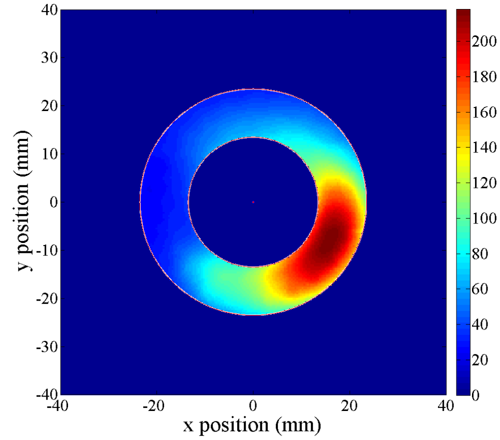

Figure 8. Color image corresponding to left raw image. Scale is in mm. A mask was applied to delete light outside the channel boundaries that are indated by the solid lines.

B. High-speed camera

Two version of the Phantom high-speed digital camera from Vision Research have been employed in this work: the v2512 and the v1612. A speed up to 1 M frame-per-second (fps) can be achieved with the two cameras at reduced resolution. The maximum image resolution is 1280×800 pixels. The minimum exposure time is 1 μs. Images are saved in grayscale with a 12-bit depth per pixel that yields high dynamic range and excellent image quality.

For high-speed camera imaging of the two configurations of the ISCT200 Hall thruster, the camera has been aligned on the thruster axis and positioned 2 m away from the channel exit plane. Imaging of the thruster front panel is performed through a 5 mm thick quartz window.

IV. Image processing

A. Image transformation

A very large set of images of Hall thruster plasma discharge has been acquired during several experimental campaigns. More than 200 videos have been recorded and the total data set size amounts to about 460 Go. Before processing images, it is however necessary to adatp the movie and image format for computer analysis.

Several high-speed camera video sizes have been tested. A good compromise between the file size, which defines the computation time, and the number of recorded images that allows for a good statistics during data treatment was found to be in the range [2000–10000] images. Most videos treated in this work comprise 2000 frames and the corresponding file size is around 300 Ko according to camera resolution.

The Phantom camera saves raw video in the *cine* format that includes all images and related information. The first step consists in transforming the *cine* images into TIFF (Tagged Image File Format) images. TIFF is a common computer file format for storing raster graphics images. A TIFF file includes the images as well as tags (size, definition, image-data arrangement, applied image compression...). In this work raw *cine* images have been converted into 8-bit grayscale images such that each pixel is represented by one 8-bit byte. The maximum number of gray shades, or colors, is then $2^8 = 256$. The size of a TIFF video (set of 2000 images) is typically 130 Mo. Notice the gain of the camera must be adjusted in such a way the light intensity never saturates, i.e. the pixel intensity never reaches 256.

A MATLAB® (MATrix LABoratory) program, developed in-house, is employed for image processing and subsequent data treatment. In order to facilitate and to speed-up data processing, each TIFF video must be converted into a 3D matrix of the form *nb_pixels* × *nb_pixels* × *nb_images*. A Wiener filter is used for noise reduction before copying an image into the matrix. Figure 7 shows a 8-bit gray scale filtered image of a rotating plasma inhomogeneity in the discharge of the ISCT200 Hall thruster in Wall-Less configuration

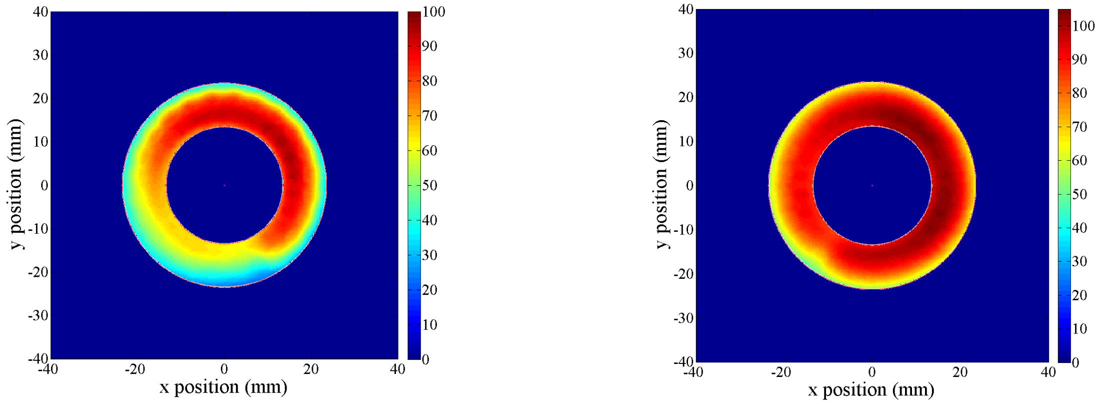

Figure 9. Mean image of the ISCT200-WL Hall thruster operating at 110 V and 1.2 mg/s with a large anode electrical connection (left) and a miniaturized connection (right).

firing at 110 V, 1.2 mg/s-Xe and 0.97 A. The high-speed camera settings were: 100000 fps (10 μs time interval), 7.66 μs exposure time, 256×256 pixel resolution.

The next step is the transformation of pixels into *mm* to get the real rotating structure size and speed. To achieve this step it is necessary to find the thruster center and the channel inner and outer boundaries as well. For simplifying image processing, the ligth recorded outside the thruster channel boundaries is maksed, or in other words, the light intensity is set to $2^0 = 1$ outside the channel. Finally, the grayscale is converted into a color scale,which make easier the plasma structure visualization by the naked eye.

Figure 8 shows a color image obtained from the previous black and white image (Fig. 7). The x and y axis are in mm and a mask has been applied to remove light outside the channel boundaries.

B. Mean image

A mean image of the thruster discharge is obtained by averaging the light intensity over the image number in the recorded series. The mean image provides useful information. Defects in the gas flow, in the anode properties or in the discharge current collection are directly revealed by the mean image. In the case of a stable and periodical dynamics of the rotating structure, the mean light intensity is homogeneous in the azimuthal direction and radial gradients do not depend on the angle. Departure from this ideal picture indicates a complicated and non-periodic structure dynamics.

Figure 9 shows two mean images of the ISCT200 Hall thruster in Wall-Less configuration firing at 110 V discharge voltage and 1.2 mg/s xenon mass flow rate. The left picture reveals a heterogeneous light intensity distribution with a low light amount around $\theta = -90°$. The left image is quite homogeneous in the θ direction, although light intensity is slightly larger on the right side. A small defect is visible at $\theta = -130°$, the location of the gridded anode electrical connection. The only difference between these two series is the size of the electrical connection between the wire and the gridded anode. Due to the relatively large anode temperature, the wire cannot be welded and a mechanical connection is needed. In the first case (left image), the connection was relatively big and it perturbed the gas flow, which explains the low plasma density in the connection region. The connection was then modified and schrunk to minimize disturbances of the neutral gas flow distribution downstream of the gridded anode (right image). Notice in the first case the structure dynamics was found to be more chaotic and the plasma inhomogeneities hardly moves through the region of low gas density.

All ISCT200-WL videos examined in this work have therefore been recorded with a small anode electrical connection.

C. Rotating structure image series

A time series of processed images of the ISCT200-WL thruster plasma discharge is shown in Fig. 10. The Hall thruster was operated at 110 V applied voltage, 1.3 mg/s Xe mass flow rate and 1.16 A discharge current. The camera frame rate was set to 100000 (time interval = 10 μs) and the exposure time was 7.66 μs.

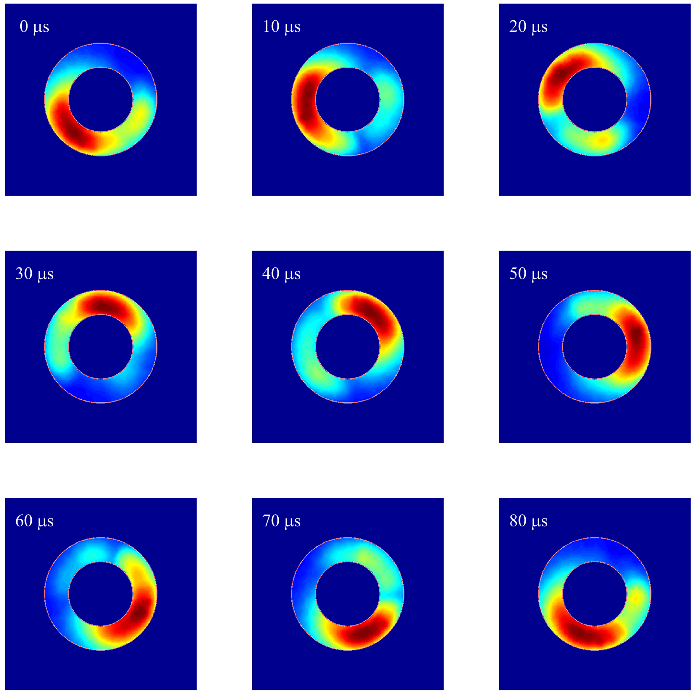

Figure 10. Time series of processed fast camera images of the ISCT200-WL thruster (110 V, 1.2 mg/s).

A well-defined structure propagating clockwise, i.e. in the $E \times B$ drift direction, is visible in Fig. 10. The bright region (in red according to our colorbar) corresponds to the plasma inhomogeneity, that means a region with a high plasma density. As light is linked to excitation processes by electron impact, a luminous zone images a zone with a high electron density and electron temperature. Only one structure is present: the discharge is said to be in the $m = 1$ mode, following the definition proposed by McDonald and co-workers.[14] The mode number m indicates the number of structures simultaneously present in the discharge. The $m = 0$ mode corresponds to the so-called Hall thruster breathing mode.[35,40–42] In that peculiar case, the entire discharge flashes in unison.

The structure size is about 1/4 of the channel cross-section area. Its length is about 1/4 of the channel circumference and its width is the channel width. However, as the camera exposure time is relatively long, the structure dimensions are certainly a bit overestimated.

As can be seen in Fig. 10, it takes about 90 μs for the structure to travel one turn. The rotation frequency f is therefore around 11.1 kHz. The rotation velocity is defined as:

$$v = 2\pi r f = \pi d f, \tag{1}$$

where r and d are the channel mean radius and mean diameter, respectively. The structure velocity is then 1290 m/s. The angular velocity ω is given by:

$$\omega = \frac{v}{r} = 2\pi f. \tag{2}$$

The angular velocity is equal to 69743 rad/s. The wavelength associated with the plasma inhomogeneity reads:

$$\lambda = vT = \frac{v}{f}, \tag{3}$$

where T is the rotation period. Here λ is the channel circumference as $m = 1$. A more general definition of the propagation velocity and wavelength accounts for the mode number:

$$v_m = \frac{2\pi r f_m}{m} \qquad \text{and} \qquad \lambda_m = \frac{v_m}{f_m} = \frac{2\pi r}{m}, \tag{4}$$

where the subscript m refers to the value of m.

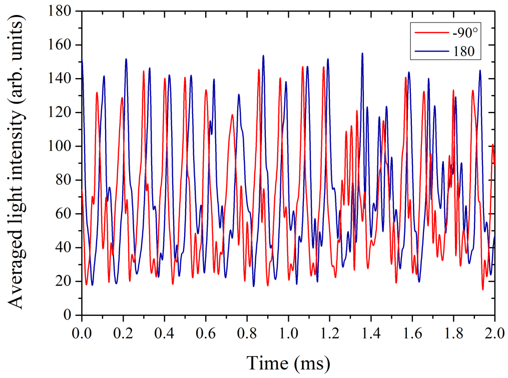

Figure 11. Temporal evolution of the light intensity at -90° and 180° angles. ISCT200-WL thruster operating at 110 V and 1.2 mg/s.

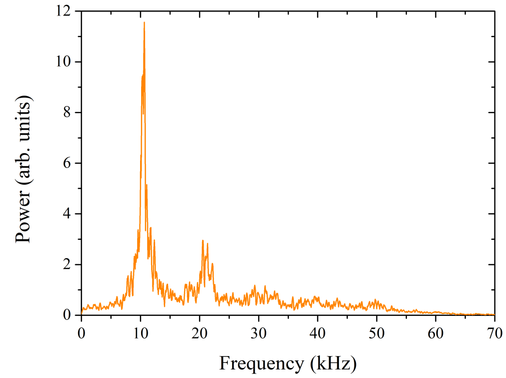

Figure 12. Power spectrum of the light intensity trace at -90°. ISCT200-WL thruster operating at 110 V and 1.2 mg/s.

D. Video analysis

Viewing of a series of images allows to assess several quantities like the plasma structure sizes, the rotation period and the mode number. However, to get accurate values of structure characteristics and to capture detailed information about the dynamics, the analysis of time sequences of digital images has to be performed with mathematical tools and sophisticated algorithms.

The MATLAB® numerical computing environment has been used in this study to analyse images and videos. MATLAB® allows matrix manipulations, which is the basic form of a plasma inhomogeneity video after transformation, as explained in section A. A good introduction to image processing with MATLAB® can be found in reference.[43] In the next paragraphs, several methods for computing the plasma structure velocity and the rotation frequency are presented and discussed. The video of the ISCT200-WL thruster firing at 110 V, 1.3 mg/s and 0.97 A is used as a test case. Camera settings are: 100000 fps and 256×256 resolution.

1. Light intensity temporal evolution

The evolution in time of the light intensity can be observed at any location, i.e. one pixel at (r, θ) coordinates, in the region defined by the channel boundaries. To reduce the statistical noise, it is nonetheless preferable to integrate or to average the light intensity along a radius between the inner and outer boundaries for each frame. One therefore obtains the mean light intensity at a given azimuthal angle and at a given time. At least two angles must be considered to distinguish between oscillations in the azimuthal direction (rotating structures) and in the axial direction (breathing mode). In case of instabilities propagating in the θ direction, a clear phase-shift or time-shift exists between light waveforms at various angles. Figure 11 shows the temporal evolution of the light intensity at -90° and 180° computed from the video of the ISCT200-WL thruster at 110 V. The two traces are quite similar. Besides there is an almost constant time-shift between the two traces, which reveals propagation in the azimuthal direction. The sign of the time-shift agrees with a clockwise propagation of the structure. The phase difference is around $\pi/2$ as expected.

The rotation speed can be computed by finding all peaks of a given waveform. The peak location gives the mean period and the associated standard deviation. The use of a threshold in the light intensity is needed to isolate the main peaks. A minimum distance between peaks, in the order of the most probable rotation period, can also be incorporated into the program. A more accurate method would consist in computing the phase-shift between light intensity time series obtained at different angles. This method requires, however, to well identify the peaks. It is not yet implemented into the code.

The rotation velocity can also be retrieved from the Fourier transform of the time series. A FFT algorithm is used. The Parseval's theorem, which warrants energy conservation in time and in the frequency space, is verified after each calculation of the power spectrum. Figure 12 shows the power spectral density of the time series of the light intensity at -90°. The dominant frequency is 10650 Hz, which corresponds to a 94 μs

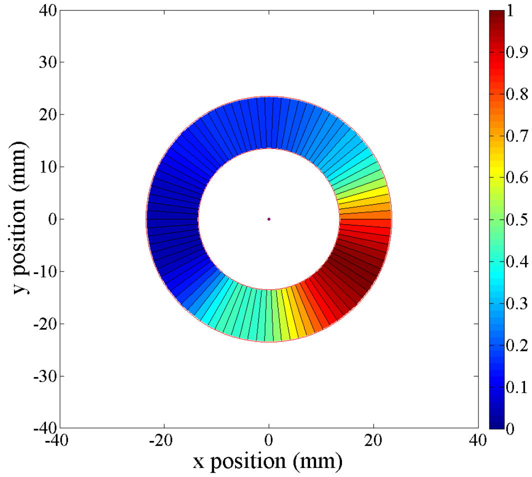

Figure 13. Normalized segmented image (90 slices) of image shown in Fig. 8. ISCT200-WL thruster operating at 110 V, 1.2 mg/s and 0.97 A.

time period in agreement with the period found from the frame sequence in Fig. 10.

2. Image segmentation

The light intensity distribution inside the area delimited by the annular channel walls can be divided into discrete angular segments or slices with n pixels.[16] The pixel intensity is averaged in each slice. A slice is then defined by only two quantities: angle and intensity, or color. Image segmentation is a way to reduce a 3D problem (r, θ, pixel intensity) into a 2D problem (θ, mean intensity). The number of slices can be chosen betwen 2 and 360. There is, however, a minimum number below which the plasma structure is not well identified because intensity changes are too smoothed. In our case, this number is around 60 and a segmented image is typically cut into 100 slices. A normalized segmented image of the ISCT200-WL thruster image presented in Fig. 8 is shown in Fig. 13. The channel area is divided into 90 slices. The corresponding azimuthal profile of the segment intensity is shown in Fig. 14.

The plasma inhomogeneity angular position is defined as the azimuthal angle of the slice having the highest intensity. Following this approach, the structure is at -34° in Fig. 13. The rotating velocity is then determined from the structure angular position of two consecutive frames. To get an more accurate value of v, two constraints are included into the algorithm. Firstly, to eliminate sporadic "jumps", the difference between two angles cannot exceed a certain threshold, half a circle, i.e. 180°, here. Secondly, structure moving in the wrong direction, i.e. in a counterclockwise direction in the current example, are not taken into account. The treatment of each video frame therefore leads to a distribution of the rotation velocity. The plasma inhomogeneity propagation velocity distribution function is shown in the form of a bar graph in Fig. 15 in the case of the ISCT200 thruster in WL configuration operating at 110 V in the NExET chamber. The mean and most probable velocity associated with the distribution are 1213 m/s and 1279 m/s, respectively. Table 2 gives the mean and most probable velocity as a function of the number of slices. As can be seen, the dispersion is small, meaning the slice number has a little influence on the structure velocity.

Table 2. Mean and most probable rotation velocity as a function of the slice number. ISCT200-WL thruster operating at 110 V.

Slice number	40	60	90	180	360
v_{mean} (m/s)	1289	1303	1213	1220	1218
v_{mp} (m/s)	1162	1569	1279	1337	1221

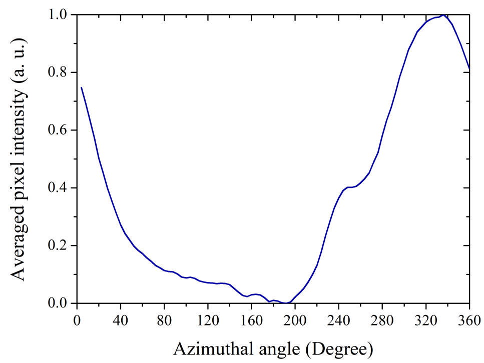

Figure 14. Azimuthal profile of slice intensity ($n = 90$). ISCT200-WL thruster operating at 110 V and 1.2 mg/s.

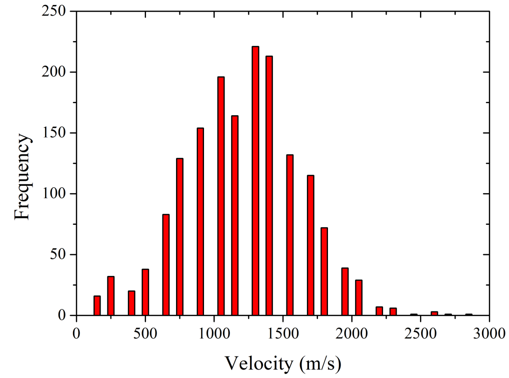

Figure 15. Velocity distribution function computed from analysis of segment images. ISCT200-WL thruster operating at 110 V and 1.2 mg/s.

3. Spoke surface

Another way of determining the plasma structure propagation velocity is to use the so-called "spoke surface".[14,16] Taken together, azimuthal profiles of slice intensity previously described form a 2D matrix termed the "spoke surface". This matrix has columns equal to the number of azimuthal sclices (angle) and rows equal to the number of video frames (time). The matrix element defined by the standard (row, column) indexing scheme is the slice intensity at (t, θ). Figure 16 is a contour plot of the spoke surface associated with the segmented image in Fig. 13. Clear striations are visible in the figure. Angled parallel striations in the spoke surface correspond to modes propagating azimuthally in time. The negative slope of the striations is in agreement with rotation in the clockwise direction. In the case of breathing oscillations ($m = 0$ mode) instead of azimuthal instabilities, the striations would be vertical.

The rotation velocity can be inferred from the slope of the striations. The striations are automatically detected in our program. However, the algorithm is faster and more accurate when the color spoke surface is transformed into a binary (1-bit) image, i.e. an image that has only two possible values for each pixel. A global threshold (level) has to be used to convert an intensity image to a binary image. The Otsu's method

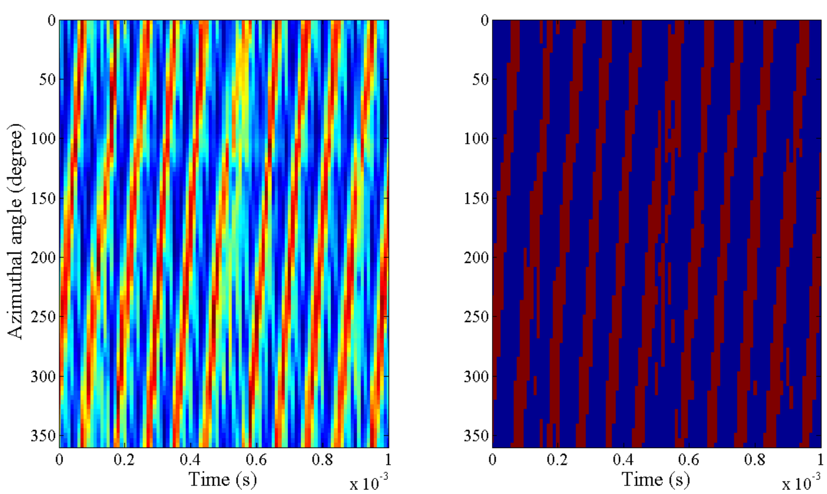

Figure 16. Spoke surface and corresponding binary image. ISCT200-WL thruster operating at 110 V, 1.2 mg/s and 0.97 A.

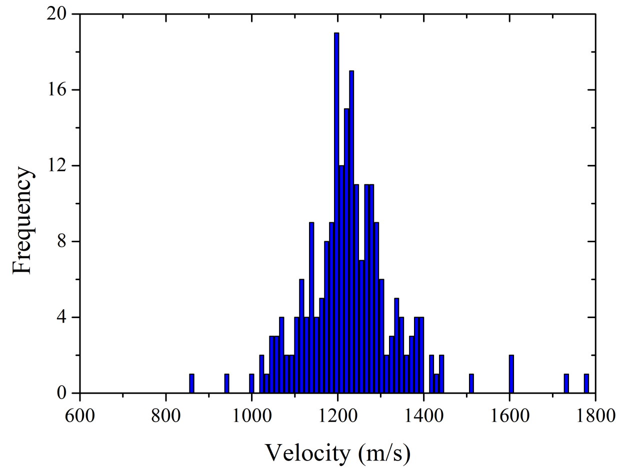

Figure 17. Velocity distribution computed from spoke surfaces. ISCT200-WL thruster operating at 110 V, 1.2 mg/s and 0.97 A.

has been applied here: the threshold is chosen to minimize the intraclass variance of the black and white pixels. A binary image of a spoke surface is shown in Fig. 16. A linear fit through each striation can be used to determine the structure velocity for each turn. Yet, another approach, easier to numerically implement, has been preferred. Connected components (segments or lines) are isolated in the binary image and the x and y coordinates of their center of mass are found. The striation direction, or slope, is given by a set of successive centers of mass. The distribution of velocities obtained from the spoke surface in the case of the ISCT200-WL Hall thruster fired at 110 V is given in Fig. 17. The most probable velocity is equal to 1220 m/s.

The value of the plasma inhomogeneity rotation velocity obtained with the various methods, as well as the associated frequency, is given in Tab. 3. As can be seen, values are very close to one another. The mean velocity is 1251 m/s and the standard deviation is 31 m/s. The image segmentation method has been used to extract plasma structure parameters from videos of both the ISCT200 and the STP100 Hall thrusters.

V. Rotating spoke properties: Standard configuration

A. Images

Images of the plasma discharge of the ISCT200 Hall thruster in standard configuration have been acquired with the high-speed camera for discharge voltages ranging from 110 V to 400 V at a xenon mass flow rate of 1.2 mg/s up to 250 V and a mass flow rate of 1 mg/s above. The camera frame rate was set to 130000 fps and the exposure time was 6.19 μs. Figure 18 shows a series of nine consecutive digital images of the ISCT200-ST thruster fired at 120 V. All video frames have been cleaned with a Wiener filter and cropped to remove pixels

Table 3. Rotation velocity and frequency from the various methods. ISCT200-WL thruster operating with xenon at 110 V and 1.3 mg/s.

Method	Velocity (m/s)	Frequency (Hz)	Comments
Visual inspection	1290	11100	Not accurate
Intensity trace	1229	10576	2 angles
Trace FT	1238	10649	
Segmented image	1279	11003	90 bins ; $v_{\rm mp}$
Spoke surface	1220	10495	striation slope

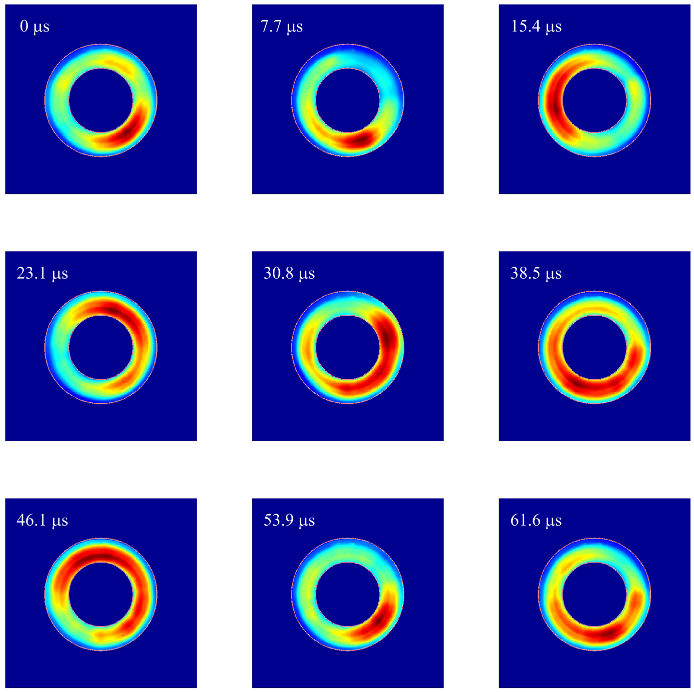

Figure 18. Time series of processed fast camera images of the ISCT200 thruster in standard configuration (120 V, 1.4 mg/s, 0.84 A).

outside the annular channel boundaries. A well-defined rotating plasma inhomogeneity in the $m = 1$ mode can be observed in this figure. The plasma structure rotates in the clockwise direction, i.e. in the $E \times B$ electron drift velocity direction. The image sequence of Fig. 18 indicates a rotation period around 55 μs, a frequency equal to 18180 Hz and a propagation velocity in the azimuthal direction equal to 2115 m/s. The rotation velocity appears to be much larger than the velocity measured in the Wall-Less configuration. Finally it is worth noticing that the plasma structure dynamics is less stable, or less periodical, in the standard configuration of the 200 W Hall thruster. The dispersion in velocity is relatively large and the stucture dimensions changes in the course of the rotation, as illustrated in the frames shown in Fig. 18.

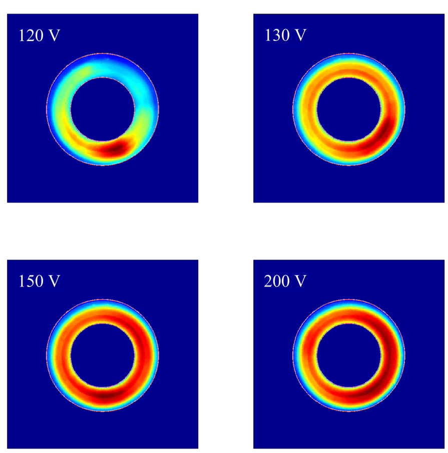

Figure 19. Digital images of the ISCT200 thruster in standard configuration at various discharge voltages (1.2 mg/s).

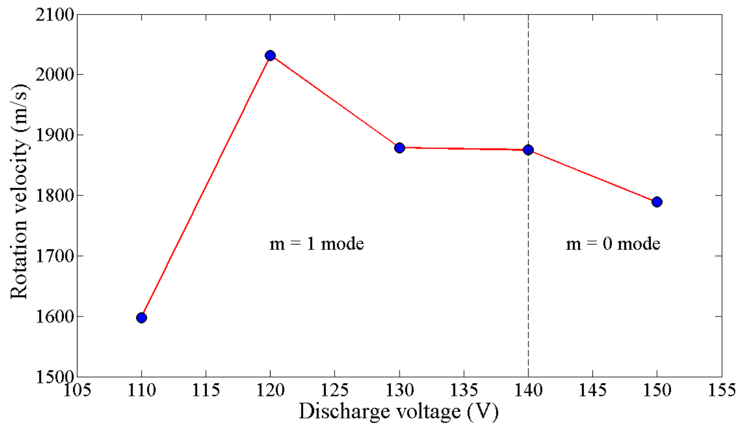

Figure 20. Plasma inhomogeneity rotation velocity against discharge voltages. ISCT200-ST thruster fired at 1.2 mg/s.

The influence of the applied discharge voltage upon the plasma inhomogeneity is exemplified in Fig. 19. A $m = 1$ mode structure has been observed up to $U_d \approx 150\,\text{V}$. Above this voltage the discharge is in the $m = 0$ mode and only the breathing oscillation remains. The length of the plasma structure increases when U_d is ramped up, see Fig. 19. The transition between the $m = 1$ and $m = 0$ modes occurs when the structure size matched the annular channel perimeter.

B. Rotation velocity

The structure rotation velocity was determined between 110 V and 150 V using the intensity trace and the image segmentation methods as well. The xenon mass flow rate was fixed at 1.2 mg/s. Results of image processing are given in Tab. 4. The velocity magnitude depends on the applied technique: for each thruster discharge voltage, the difference in velocity is around 200 m/s. A possible uncertainty source is the large size of the structure. The two techniques, however, indicate the velocity increases with U_d up to 140 V. At this voltage, the plasma discharge probably enters the $m = 0$ mode regime: the inhomogeneity dissapears and the breathing instability dominates.

A plot of the plasma structure rotation velocity as a function of the voltage is displayed in Fig. 20. The velocity corresponds to the most probable velocity calculated with the image segmentation method. There is an apparent increase in the velocity up to $U_d = 140\,\text{V}$. A deeper investigation is however necessary to confirm this point.

C. Breathing oscillations

As previously explained, in the standard configuration, the plasma discharge of the ISCT200 Hall thrusters switches from the $m = 1$ mode to the $m = 0$ mode for an applied voltage around 150 V. Figure 21 shows the spoke surface of the ISCT200-ST thruster operating at 200 V and 1.2 mg/s. As can be seen the striation are

Table 4. Rotation velocity in the plasma discharge of the ISCT200-ST thruster operating at 1.2 mg/s.

Voltage (V)	Velocity (m/s)	Velocity (m/s)
	Segmentation	Int. trace
110	1598	1825
120	2031	2187
130	1879	2366
140	1875	2384
150	1789	2403

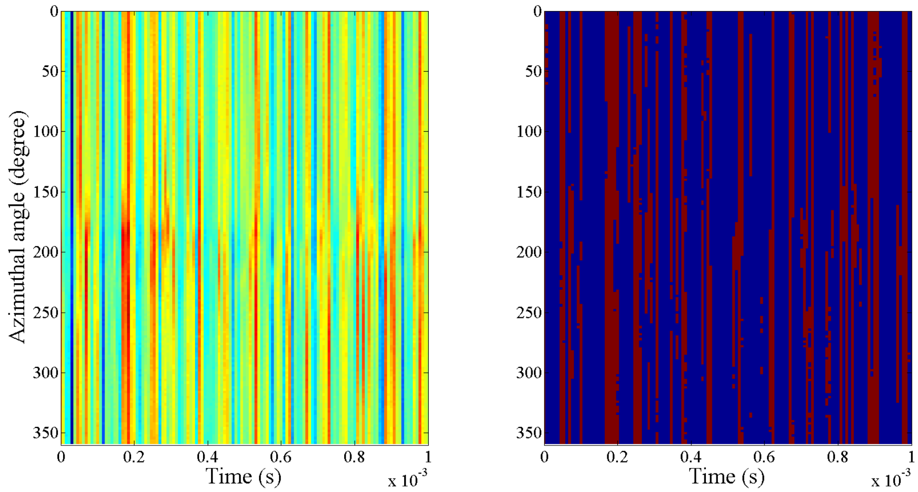

Figure 21. Spoke surface of the ISCT200-ST thruster fired at 200 V and 1.2 mg/s. Raw data (left) and corresponding binary image (right).

vertical, the signature of the breathing oscillation. The breathing mode frequency can be assessed from the binary image. A visual inspection gives $f \approx 10\,\text{kHz}$.

A more accurate calculation of the breathing oscillation frequency rests upon the image mean intensity. The mean intensity of each video frame is computed by averaging the intensity of pixels situated inside the annular channel area. The breathing frequency is then assumed to be the main frequency of the Fourier power spectrum of the resulting intensity trace. Notice the time-varying frame mean intensity should image to a large extent the thruster discharge current waveform. The evolution of the breathing mode frequency with the discharge voltage is shown in Fig. 22 for the ISCT200-ST thruster at 1.2 mg/s mass flow rate. The frequency gradually increases with U_d.

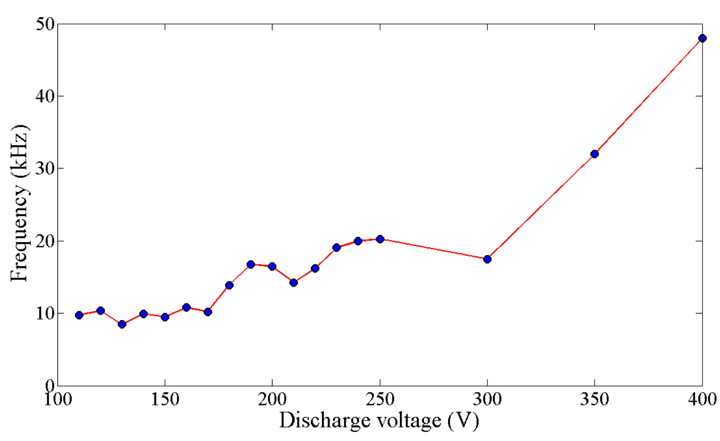

Figure 22. Breathing mode frequency against discharge voltage. ISCT200-ST thruster fired at 1.2 mg/s.

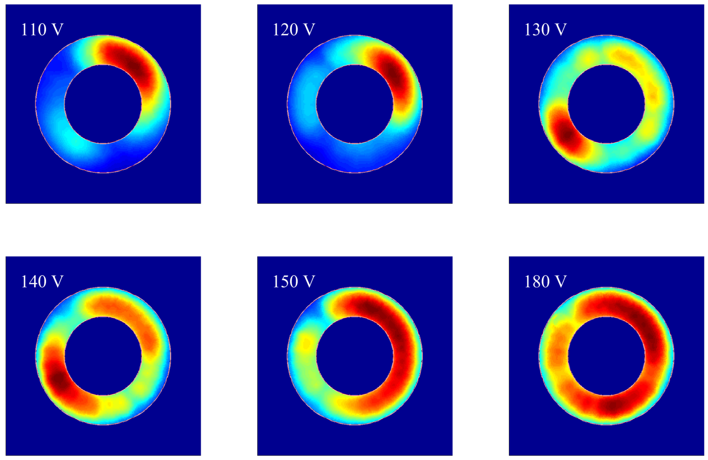

Figure 23. Digital images of the ISCT200 thruster in wall-less configuration at various discharge voltages (1.2 mg/s).

VI. Rotating spoke properties: Wall-less configuration

A. Impact of the applied voltage

Images of the plasma discharge of the ISCT200 Hall thruster in wall-less configuration have been acquired with the high-speed camera for discharge voltages ranging from 110 V to 350 V at a xenon mass flow rate of 1.2 mg/s. The camera frame rate was set to 100000 fps and the exposure time was 7.66 μs. A series of consecutive digital images of the ISCT200-WL thruster fired at 110 V is displayed in Figure 10.

The plasma structure rotates in the clockwise direction, i.e. in the $E \times B$ electron drift velocity direction, whatever the applied voltage. The influence of the applied discharge voltage upon the plasma inhomogeneity shape is exemplified in Fig. 23. A $m = 1$ mode structure has been observed up to $U_d \approx 200$ V, with a few occurrences of the $m = 2$ mode, especially above 130 V, see Fig. 24. However, the structure stops rotating at about 150 V. Between 110 V and 130 V, the plasma inhomogeneity is clearly-defined with sharp boundaries. Besides its dynamics is stable and quasi-periodical with a relatively low dispersion in velocity. From 150 V the breating oscillation dominates. A distinct $m = 0$ mode with a homogeneous discharge in the azimuthal direction is observed above 200 V. As with the standard configuration, the length of the plasma structure increases when U_d is ramped up in WL geometry. Figure. 23 illustrates the change in size of the structure with the applied voltage.

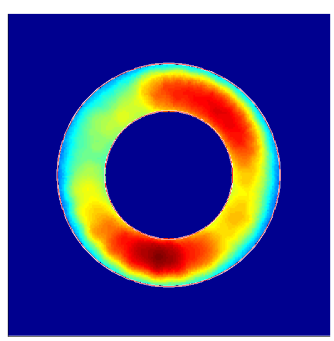

Figure 24. Plasma inhomogeneities in the $m = 2$ mode. ISCT200 thruster in wall-less configuration (150 V, 1.2 mg/s).

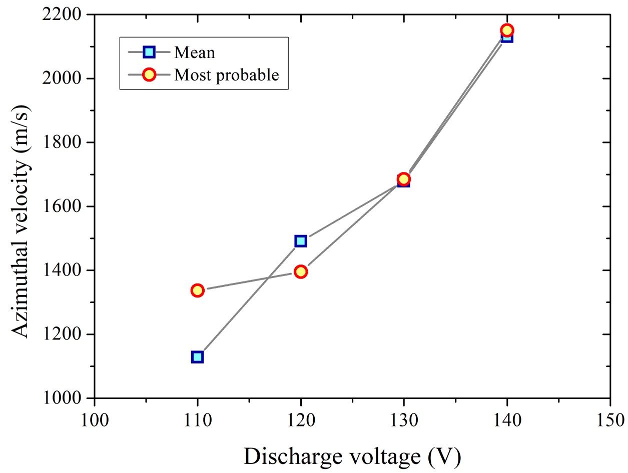

Figure 25. Plasma inhomogeneity rotation velocity against discharge voltage for the ISCT200-WL thruster (1.1 mg/s).

A plot of the plasma structure rotation velocity as a function of the voltage is displayed in Fig. 25 for the WL configuration. The velocity has been determined by means of the image segmentation method. Both the mean and the most probable velocities are shown in the figure. The two values are very close, that means the VDF is symmetrical. As with the standard configuration, there is an apparent increase in the velocity up to $U_d = 140\,\text{V}$. The velocity magnitude is nonetheless slightly lower in the WL configuration compared to the conventional configuration, see Fig. 20.

The breathing oscillation frequency has been assessed using the image mean intensity approach, see paragraph C. The evolution of the breathing mode frequency with the discharge voltage is shown in Fig. 26 for the ISCT200 thruster in wall-less configuration. The xenon mass flow rate was set at 1.2 mg/s. As with the ISCT200-ST thruster, the breathing frequency gradually increases with U_d. The frequency is the highest at 210 V with the WL architecture.

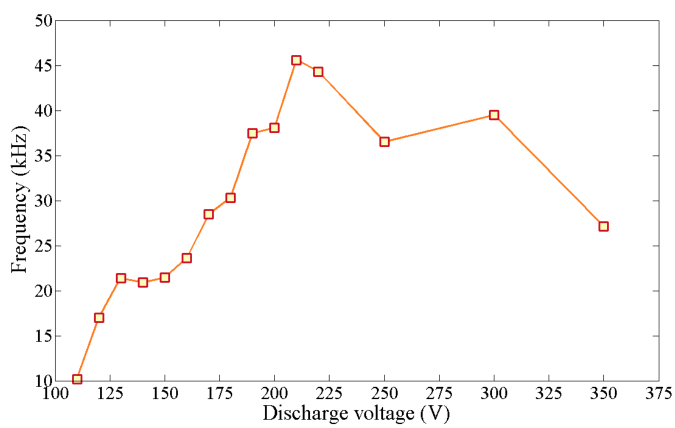

Figure 26. Breathing oscillation frequency against discharge voltage for the ISCT200-WL thruster (1.2 mg/s).

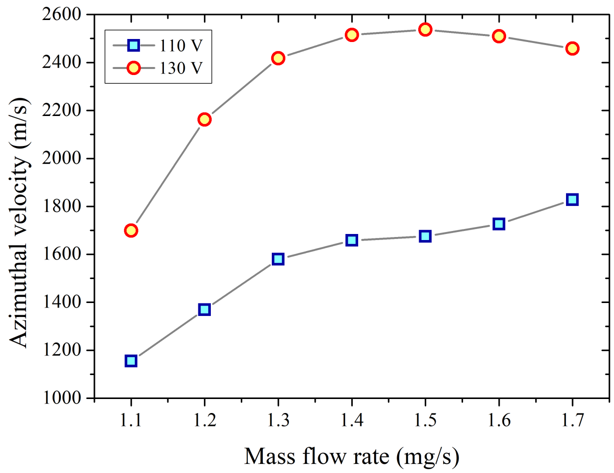

Figure 27. Azimuthal velocity of the plasma structure as a function of the xenon mass flow rate. ISCT200-WL thruster at 110 V (square) and 130 V (circle).

B. Impact of the propellant mass flow rate

The effect of the xenon mass flow rate upon the plasma structure azimuthal velocity has been investigated with the ISCT200 Hall thruster in wall-less configuration. The high-speed camera settings were: 250000 fps, 128×128 image resolution and 3.286 μs exposure time. The thruster has been fired at two distinct discharge voltages, namely 110 V and 130 V. The propellant mass flow rate has been varied in the range [1.0 − 1.7] mg/s. The limits were given by the stability of the plasma discharge.

A well-defined plasma structure in the $m = 1$ mode is observed most of the time whatever the gas flow rate for the two voltages. A few occurrences of the $m = 2$ mode have been seen. The structure always propagates in the clockwise direction, i.e. in the $E \times B$ drift direction. The azimuthal velocity has been computed using the segmentation methode (90 bins). The mean velocity of the distribution is plotted in Fig. 27 as a function of the mass flow rate. The velocity increases with Φ over the entire range for $U_d = 110$ V. When U_d is set to 130 V, the velocity first increase and then it reaches a plateau around 2500 m/s. Changes in the rotation velocity with the gas flow rate demonstrate the influence of the neutral gas density upon the plasma inhomogeneity dynamics.

C. Influence of the cathode heater current

High-speed imaging has been carried out while varying the cathode heater current between 16 A and 19 A. The opertaing conditions of the ISCT200-WL Hall thruster were: 130 V and 1.3 mg/s. A plot of the plasma inhomogeneity roation velocity is displayed in Fig. 28. The heater current has a clear impact upon the velocity: the velocity increases quickly when the current is ramped up. The drop at 19 A is not explained. The discharge current increases gradually from 1.1 A to 1.2 a when I_c is changed from 16 A to 18.5 A. It drops to 1.1 A at 19 A, which may be a sign for a change in cathode discharge mode, i.e. a transition from the so-called spot mode (small and well defined plume, low current oscillations) to the so-called plume mode (diffuse plume, large current oscillations).[20]

The plasma structure always rotates clockwise (in the E×B direction) but at 16 A where counterclokwise rotation is sometime observed. The structure is most often in the $m = 1$ mode. A few occurences of the $m = 2$ mode have been seen, but there is no apparent correlation with the cathode heater current intensity. The rotating spoke size seems smaller at 16 A.

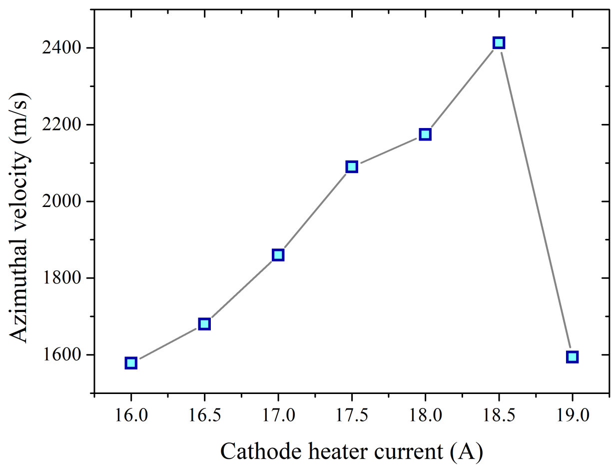

Figure 28. Plasma inhomogeneity rotation velocity (mean value) against the cathode heater current for the ISCT200-WL thruster (130 V, 1.3 mg/s).

VII. Time evolution of the ion VDF

A. Principle of time-resolved LIF

Time-resolved laser induced fluorescence spectroscopy (TR-LIF) relies on the same principles as the more classical time-averaged LIF. However the fluorescence signal needs to be recorded and correlated with some periodic phenomenon occuring in the thruster discharge.[37,38]

The challenging part is that after laser excitation in the near infrared of the Xe^+ ion optical transition, only $\sim 10^5$ photons at the 542 nm fluorescence wavelength are collected per second. About 90% of those photons are background photons, i.e. spontaneous plasma light emission, and do not originate from the laser beam excitation. This means that, for phenomena with characteristic frequencies in the ten of kilohertz range, there is only in the order of one LIF photon collected per period. To reconstruct a time-dependent ion VDF with an acceptable signal-to-noise ratio and temporal resolution the signal needs to be accumulated over tens of thousands of cycles at the very least. To keep a manageable acquisition time only a dozen or so wavelengths, or velocity groups, are probed.

So far TR-LIF in Hall thrusters has been used mainly to study the breathing mode instabilities.[37,44–47] Different methods have been used to accumulate the fluorescence signal. The method used at ICARE relies on two key components. Firstly, a voltage modulation system is used to stabilize the breathing mode oscillation both in phase and frequency. This creates repeatable identical oscillations which make it easy to accumulate photons over a long period of time. The second critical part of the measurement system is a MCS-PCI multichannel scaler acquisition card from Ortec, used to count and accumulate photons. This card accumulates pulses corresponding to single photon events detected by a low dark-noise current photomultiplier tube. The accumulation sequence is triggered by the modulation circuit. An histogram is then constructed by accumulating over hundreds of thousand of cycles. Measurements are realized with and without the laser beam to statistically distinguish between background and LIF photons. The acquisition is performed at several wavelengths to reconstruct the evolution over time of the ion VDF. Notice that the optical train and the detection branch are identical for time-averaged and time-resolved LIF measurements. Only the signal detection part is different: phase-sensitive detection with a lock-in amplifier and pulse counting, respectively. The LIF optical bench used in this work is described in section III.

Other techniques based on heterodyne methods have been used with success.[46,47] They, however, also require either a stabilization system or a fairly stable and periodic phenomenon. Sadly our high-speed imagery study show that natural plasma inhomogeneity rotation is never perfectly stable, both in frequency and phase. In the worst cases, plasma structures can appear and disappear at seemingly random time and location. This poses a challenge for TR-LIF. Whatever method is chosen, knowledge of the plasma

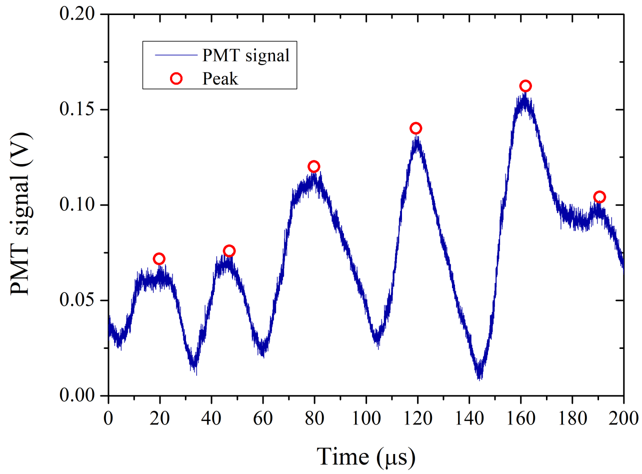

Figure 29. Time evolution of the light intensity at the LIF measurement location (middle of the thruster channel at -90). The peaks matches the passage of a plasma inhomogeneity.

inhomogeneity position at a specific time is required. As described in the following paragraphs two approaches have been investigated.

B. Discharge stabilization

Attempts were made to stabilize the dynamics of rotating plasma inhomogeneities in the external discharge of the ISCT200 Hall thruster in the wall-less configuration with the same system as the one used for the breathing oscillation studies, see[44] and references herein. The objective there was to force the rotation of a single plasma structure at a well defined frequency and with a stable phase.

In order to control the rotation, a sinusoidal frequency-tunable potential is applied between the cathode igniter and the negative pole of the cathode. To efficiently transfer energy to the discharge, the modulation frequency has to correspond to a resonance of the system. The modulation frequency is then set to the observed rotation frequency between 12 and 14 kHz. The current driven through the igniter is relatively low and represents less than 10 % of the discharge current. A power of about 6 W is injected into the discharge when the thruster is fired with an input power between 100 W and 200 W.

The modulation has been applied with the ISCT200-WL thruster operated at 110 V. As explained in the preceeding section, at this voltage the dynamics of the plasma structure is pretty stable with a quasi-periodic behavior and a relatively well-defined rotation speed. Unfortunately, the attempt to stabilize the dynamics was not succesful. The discharge current waveform stayed unchanged with and without the modulation. Secondly, and more importantly, high-speed image acquisition did not reveal changes in the structure characteristics although both rotation and breathing frequencies were modified when applying the modulation.

C. Plasma inhomogeneity detection

Since attempts at stabilizing the $m = 1$ plasma inhomogeneity were unsuccessful we resorted to try to detect the inhomogeneity position more directly. One obvious way to do this would be to simultaneously acquire the LIF signal and high-speed video. However this is very quickly unpractical. The size and transfer time of the video files slow down acquisition to a point where any single ion VDF would take weeks to record and process.

Instead of looking at the whole thruster channel area we chose to have a look at the light intensity at the LIF measurement point, see Fig. 6. This was done by splitting in two the collection branch optical fiber and using a second photomultiplier tube to record the total light intensity. Notice a 10 nm bandwidth interference filter was placed in between the fiber output and the second detector to isolate the ion fluorescence line at 542 nm. Experiments were performed with the ISCT200WL thruster operating at 110 V and 1.2 mg/s.

Figure 30. Average image (left) and image corresponding to the sum of 129 frames for which a rotating spoke is detected by the LIF setup (right). ISCT200-WL thruster fired at 110 V.

The signal obtained when $m = 1$ rotating spokes are present is exemplified in Fig. 29. The light trace shows a periodic oscillation with the same frequency as the one of the plasma inhomogeneity. To confirm that this is indeed the plasma inhomogeneity passing in front of the collection branch, the light signal peaks timestamps (red circles in Fig. 29)were isolated using a simple peak detect algorithm in our MATLAB® program. We then picked the corresponding frames in the synchronized high speed video. Figure 30 (right) shows an average image built with 129 of such frames. The plasma structure is well localized, which is a good evidence that the observed peaks in the light waveform correspond to the passage of a plasma inhomogeneity.

With this method we now know when the plasma inhomogeneity passes in the LIF measurement volume. Moreover, we can know when each photon is emitted relative to the position of the plasma inhomogeneity.

D. Data acquisition

Data acquisition based on the aforementioned method is difficult. In order to capture single photon the setup has to be able to detect pulses with a ≈ 10 ns width. At the same time the fluorescence signal needs to be recorded over tens of thousands of cycles, i.e. during several seconds, to get an accurate assessment of the shape of the fluorescence signal over one cycle. In order to get both the sample rate and memory depth required, a Lecroy HD6104 oscilloscope was used instead of our MCS-PCI pulse counter. The characteristics

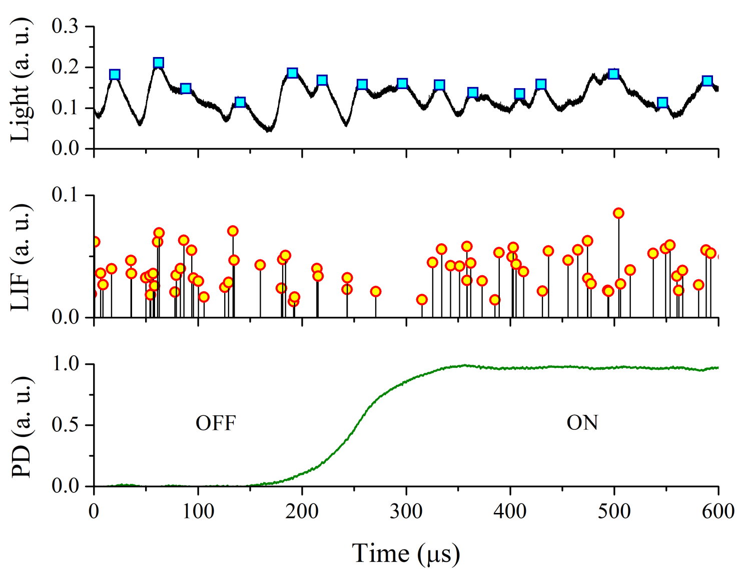

Figure 31. Light intensity (top), fluorescence photons (middle) and laser power (bottom) as recorded during a typical acquisition sequence.

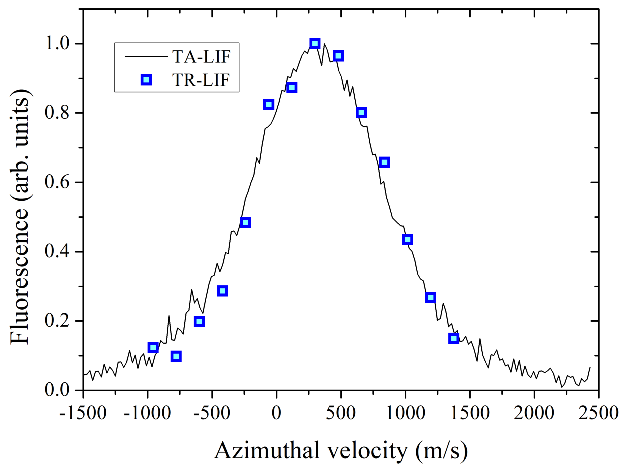

Figure 32. Normalized time-averaged Xe^+ ion VDF from time-resolved LIF measurements (square) compared to the one obtained with a standard phase-sensitive technique (line). ISCT200-WL thruster operating at 110 V.

of the oscilloscope are: 12-bit resolution, 1 GHz bandwidth, 250 Mpts per channel and 1.25 GS/s sampling rate. The oscilloscope records single photons from the two photomultiplier tubes, i.e. LIF light and total fluorescence light, as well as the signal from a fast photodiode that indicates if the laser beam propagates through the plasma (mode ON) or is suspended (mode OFF). The cw laser light modulation is achieved with a mechanical chopper set at about 1 kHz. When the laser is ON, respectively OFF, the signal includes LIF and background photons, respectively, background photons only. The LIF signal is then obtained by substracting the ON and OFF signals.[37] With a sampling frequency of 10 MHz each individual record lasts 1 second. Accumulation of about 100 s of recording is necessary to get suitable ion VDFs with a good signal-to-noise ratio. Example of raw data recorded by the oscilloscope are shown in Fig. 31. The procedure to obtain the time-dependent ion VDF at a given position consists in accumulating photons in time at a fixed wavelength, i.e. in recording the time evolution of a well-defined ion velocity group.

E. Data treatment and VDF construction

The first step in our processing is to detect each photons. To do that a peak detection algorithm is used and only peaks of a certain minimum amplitude are kept. This discrimination step allows to get rid of the detector dark noise photons. The photodiode signal is then read to find if those photons were collected

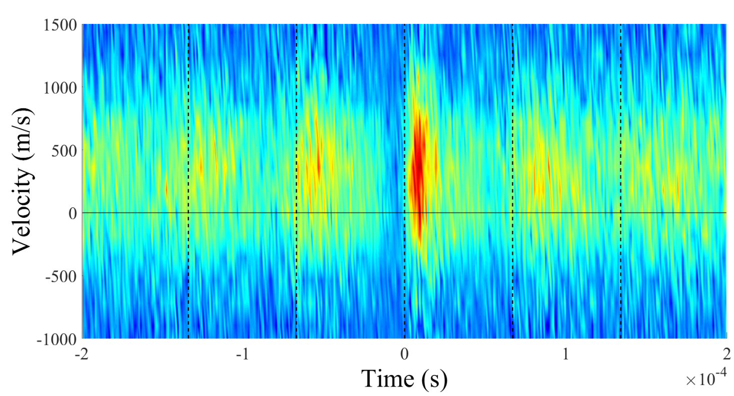

Figure 33. Outcome of data processing: Time-dependent Xe^+ VDF measured at -90°. ISCT200-WL Hall thruster fired at 110 V and 1.3 mg/s. Dashed lines indicate the rotation period.

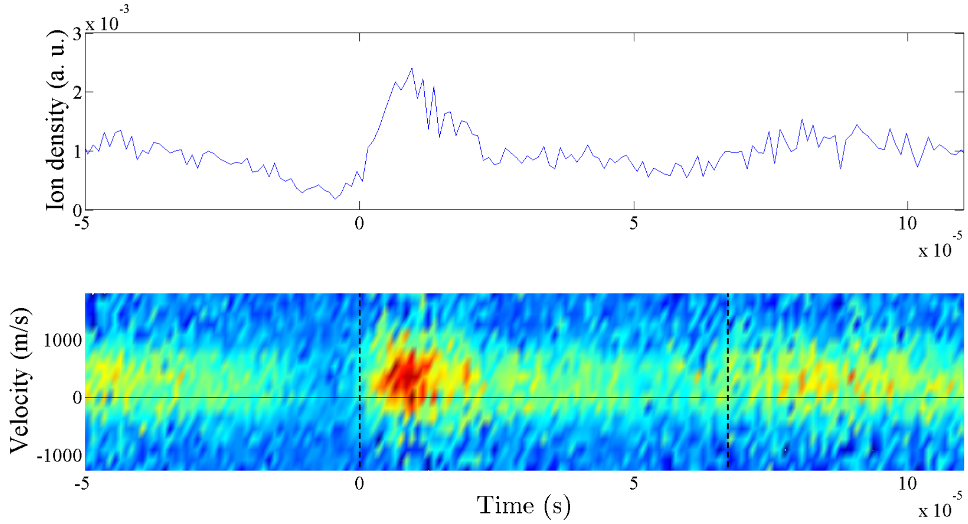

Figure 34. Time-varying distribution function of the Xe^+ ion azimuthal velocity on the channel axis at $x = 4$ mm and $\theta = -90°$. ISCT200-WL thruster operating at 110 V and 1.3 mg/s. Also shown is the relative ion density, which correspond to the LIF signal intensity. The dashed lines indicate the spoke rotation period.

during the ON or the OFF part of the laser cycle. From just this information it is possible to reconstruct the averaged shape of the ion VDF. For each wavelength we subtract the number of photons collected per second when the laser is OFF to the one when the laser is ON. We use the number per seconds instead of the total number of photon because the duration of the ON and OFF period is not exactly equal. The validity of our photon-counting technique can be established by comparing the time-averaged ion VDF obtained by means of a lock-in detector, with the one built from the temporal average of time-varying fluorescence traces. The result is illustrated in Fig. 32. As can be seen, the temporally averaged ion VDF does not depend on the fluorescence radiation acquisition device. The two ion VDFs have a very similar shape and the most probable azimuthal velocity is the same: $v_{\rm mp} = 300$ m/s. This result indicates the current statistic in terms of acquisition duration is good enough. However, the wings of the fluorescence profile are not captured in this example, that means the number of probed velocity groups has to be increased.

Once we have identified each photon with a peculiar instant in time and a corresponding laser cycle (ON versus OFF), we can determine their position in a plasma inhomogeneity rotation cycle. The temporal range of each plasma inhomogeneity passage is found suing the method previously described. From that we compute the delay between the plasma inhomogeneity and photons before and after the structure has crossed the measurement volume, this precise moment being taken as a reference. This operation provides the number of photons as a function of time for the ON and OFF modes. Subtracting the two signals for each laser wavelength gives the time-varying ion VDF. Figure 33 shows an example of the data processing outcome, i.e. the time-dependent Xe^+ ion VDF measured at -90° with the ISCT200-WL Hall thruster fired at 110 V and 1.3 mg/s. The $t = 0$ reference time refers to the detection of the plasma structure. Under these thruster operating conditions, the $m = 1$ inhomogeneity rotation period is about 70 μs, see section VI. Surprisingly, the VDF shape and the associated mean ion velocity do not change much during the structure rotation period. Our data treatment procedure allows to construct the temporal evolution of the ion VDF during several rotation periods. If the rotating spoke sizes and velocity were perfectly stable, a periodic pattern would appear in Fig. 33. However, the coherence is quickly lost and the signal weakens the further it is from the reference period due to fluctuations in time of the spoke characteristics.

F. Time-varying Xe^+ ion VDF

The time-varying ion VDF has been measured in the discharge of the ISCT200-WL thruster with a long acquisition period in order to improve the signal-to-noise ratio. Due to the required sampling rate and record length, data can quickly amount for several hundreds of gigabytes, which complicates data handling

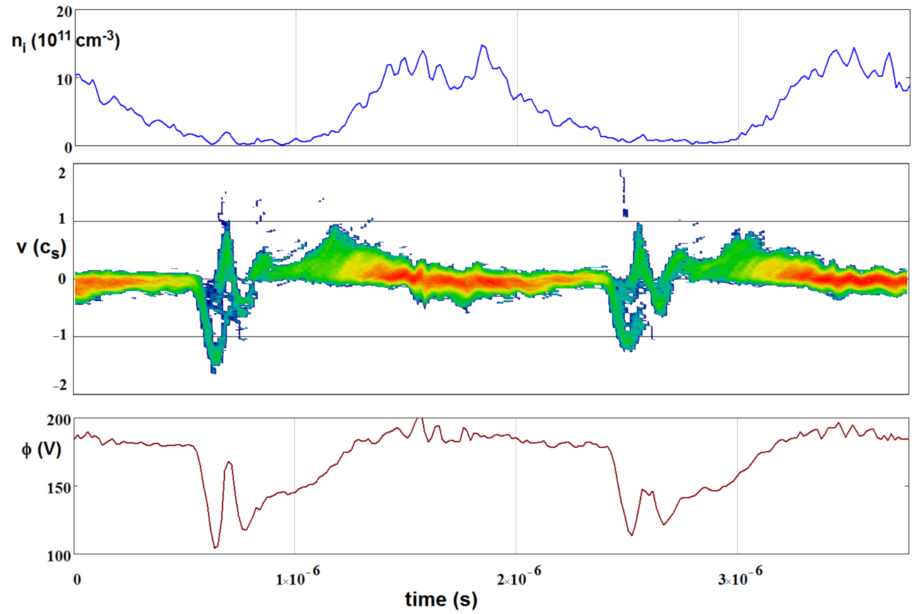

Figure 35. Simulated time-dependent ion VDF during two rotation cycles of the plasma instability (middle) at $x = 4\,\text{mm}$, $y = 0\,\text{mm}$ (on-axis) and $\theta = -90°$. The ion acoustic speed c_s is equal to 3834 m/s here. Also shown is the time evolution of the ion density (upper plot) and the time evolution of the electrical potential (lower plot). Parameters are: 175 V, 1 mg/s and $T_n = 400\,\text{K}$.

and processing. The Hall thruster operating conditions were 110 V, 1.3 mg/s and 1.15 A. Time-resolved LIF measurements of the azimuthal velocity component have been performed on the channel centerline 4 mm downstream the anode at -90° , i.e. in the ionization region, see.[21,36]

The time-dependent Xe^+ ion VDF is shown in Fig. 34 along with the relative ion density that correspond to the LIF signal intensity corrected for the laser power variation. Most ions rotate in the E×B direction (positive velocity), i.e. in the direction of the spoke motion. However, some ions propagate in the opposite direction (negative velocity) especially when the ion density is large, as can be seen in Fig. 34. The mean ion velocity does not vary much. The highest magnitude of the mean ion velocity is around +400 m/s, much below the rotating spoke velocity that reaches about 1600 m/s.

G. Simulated ion VDF

Computer simulations of the plasma discharge of the ISCT200 Hall thruster in wall-less configuration have been performed using the self-consistent 3D-3V Particle-In-Cell code STOIC (electroSTatic Optimized particle In cell). A detailed description of the STOIC code can be found in references.[48–50] Information and results about numerical simulations of the thruster are available in.[51] For this work, a specific diagnostic module has been developed and implemented into the code to enable the monitoring of the atom and ion VDF in time and space.

Figure 35 shows the simulated evolution in time of the ion density, the ion velocity distribution function in the azimuthal direction as well as the local plasma potential during two rotation cycles of the plasma structure at $x = 4\,\text{mm}$, $y = 0\,\text{mm}$ (on-axis) and $\theta = -90°$. The simulation conditions were: 1 mg/s Xe flow rate, 175 V discharge voltage and a neutral gas temperature of 400 K. In Fig. 35 the velocity is expressed as a multiple of the local ion acoustic wave speed c_s, which is equal to 3834 m/s here. As can be seen in Fig. 35, the distribution of the ion azimuthal velocity component is most often distinctly non-Maxwellian, with high-velocity tails. High-energy ions are created more specifically at the edges of the rotating spoke where strong potential gradients are present.

The measured and simulated time-dependent Xe^+ ion VDF are in relatively good agreement, although the thruster operating conditions were different, particularly in terms of applied voltage.[51] The code nevertheless reproduces the rotating spoke properties (size, mode number, drift direction) and dynamics but the $m = 1$ to $m = 0$ mode transition occurs at higher voltages around 250 V. In like manner, the simulated plasma inhomogeneity rotation velocity in the azimuthal direction is larger than the one inferred from fast camera imaging. The discrepancy may originate from scaling relations used in the PIC simulations to reduce the computational time and/or from the applied boundary conditions.

Many characteristics of the simulated ion VDF also appear on the measured distribution function. The mean Xe^+ ion azimuthal velocity is positive, i.e. in the $E \times B$ direction, with a small amplitude, much below the structure rotation velocity. Fast ions, with positive and negative velocities, are created during a short time periods. Note very fast ions that exist at the edges of the rotating spoke are not experimentally observed by LIF spectroscopy as the associated density is low, see Fig. 35. Finally, the ion density distribution along the channel mean circonfrence is well reproduced.

VIII. Conclusion

Characteristics as well as dynamics of rotating plasma inhomogeneities, often called rotating spokes, have been investigated in the low-pressure low-temperature plasma discharge of a 200 W-class permanent magnet Hall thruster in wall-less configuration with a curved gridded anode at the channel exit plane to shift the plasma discharge in the vacuum outside the dielectric channel. For comparison purposes, the Hall thruster was also operated in the standard configuration where the anode is placed at the back of the channel. The magnetic field topology was the same for the two configurations withthe highest magnitude at the channel outlet.

High-speed camera imaging combined with sophisticated image processing allowed to observe the plasma structure dynamics and to determine the mode number, the rotation frequency and the propagation velocity. For the two configurations, the $m = 1$ mode dominates at low voltages and transition from this mode to the $m = 0$ mode that corresponds to the breathing oscillation occurs around 150 V. The plasma instabilities always rotates in the $E \times B$ electron drift velocity direction. The azimuthal velocity is influenced by the applied voltage, the propellant mass flow rate and the external cathode properties. Whatever the thruster operating conditions, the rotation velocity of the plasma inhomogeneity stays below the critical ionization velocity, which is equal to 4220 m/s for xenon. The time varying Xe^+ ion velocity distribution function has been measured on the channel axis at -90° in front of the anode of the ISCT200-WL thruster at 110 V and 1.3 mg/s using a photon counting LIF spectroscopy technique. Whereas the mean ion velocity is not much affected by the rotating structure, the ion VDF reveals the presence of fast ions with positive and negative velocities during a short time period.

Numerical simulations of the rotating structure in the ISCT200-WL discharge have been performed with a 3D-3V PIC code. Several similarities have been found between experiments and simulations: the structure sizes are identical (about 1/5 of the channel mean perimeter), the $m = 1$ mode is the dominant one whatever the operating parameters, there is a transition from $m = 1$ to $m = 0$ at high voltages. Rotation frequencies and propagation velocity are, however, different: simulations give larger values. Discrepancies could originate from boundary conditions or scaling factor. The time-dependent ion VDF in the azimuthal direction has been reconstructed from the numerical data set. There is a good agreement between the simulated and the measured ion VDF. Simulations however reveal the existence of high-energy tails at the structure edges, regions of low plasma density and steep plasma potential gradients.

Acknowledgments

This research was funded by the EOARD under Grant FA9550-15-1-0281. We are profoundly indebted to Dr. Nabiha Chaumeix and her team for lending us the high-speed cameras.

References

[1] J. P. Boeuf. Rotating structures in low temperature magnetized plasmas – insight from particle simulations. *Frontiers in Physics*, 2:74:1–17, 2014.
[2] J.-P. Boeuf and B. Chaudhury. Rotating instability in low-temperature magnetized plasmas. *Phys. Rev. Lett.*, 111:155005, 2013.
[3] P. A. Redhead. Instabilities in crossed-field discharges at low pressures. *Vacuum*, 38:901–906, 1998.
[4] M. Keidar and I. I. Beilis. Electron transport phenomena in plasma devices with E×B drift. *IEEE Trans. Plasma Sci.*, 34:804–814, 2006.
[5] A. R. Pal, J. Chutia, and H. Bailung. Observation of instability in presence of E×B flow in a direct current cylindrical magnetron discharge plasma. *Phys. Plasmas*, 11:4719–4726, 2004.

[6]N. Brenning, D. Lundin, T. Minea, C. Costin, and C. Vitelaru. Spokes and charged particle transport in HiPIMS magnetrons. *J. Phys. D: Appl. Phys.*, 46:084005, 2013.
[7]J. Winter, A. Hecimovic, T. de los Arcos, M. Böke, and V. Schulz von der Gathen. Instabilities in high-power impulse magnetron plasmas: from stochasticity to periodicity. *J. Phys. D: Appl. Phys.*, 46:084007, 2013.
[8]A. Anders, P. Ni, and A. Rauch. Drifting localization of ionization runaway: unraveling the nature of anomalous transport in high power impulse magnetron sputtering. *J. Appl. Phys.*, 111:053304, 2012.
[9]A. Hecimovic. Anomalous cross-B field transport and spokes in HiPIMS plasma. *J. Phys. D: Appl. Phys.*, 49:18LT01, 2016.
[10]S. Tsikata and T. Minea. Modulated electron cyclotron drift instability in a high-power pulsed magnetron discharge. *Phys. Rev. Lett.*, 114:185001, 2015.
[11]M. E. Griswold, C. L. Ellison, Y. Raitses, and N. J. Fisch. Feedback control of an azimuthal oscillation in the E×B discharge of Hall thrusters. *Phys. Plasmas*, 19:053506, 2012.
[12]C. L. Ellison, Y. Raitses, and N. J. Fisch. Cross-field electron transport induced by a rotating spoke in a cylindrical Hall thruster. *Phys. Plasmas*, 19:013503, 2012.
[13]B. A. Jorns and R. R. Hofer. Plasma oscillations in a 6-kW magnetically shielded Hall thruster. *Phys. Plasmas*, 21:053512, 2014.
[14]M. McDonald, C. K. Bellant, B. A. St. Pierre, and A. D. Gallimore. Measurement of cross-field electron current in a Hall thruster due to rotating spoke instabilities. In *Proceedings of the 47th Joint Propulsion Conference*, AIAA paper 2011–5810, San Diego, CA, 2011.
[15]M. McDonald and A. D. Gallimore. Rotating spoke instabilities in Hall thrusters. *IEEE Trans. Plasma Sci.*, 39:2952–2953, 2011.
[16]M. S. McDonald and A. D. Gallimore. Comparison of breathing and spoke mode strength in the H6 Hall thruster using high speed imaging. In *Proceedings of the 33rd International Electric Propulsion Conference*, IEPC paper 2013–353, Washington D.C., 2013.
[17]M. J. Sekerak, A. D. Gallimore, D. L. Brown, R. R. Hofer, and J. E. Polk. Mode transitions in Hall effect thrusters induced by variable magnetic field strength. *J. Propul. Power*, 33:903–917, 2016.
[18]S. Mazouffre, G. Bourgeois, K. Dannenmayer, and A. Lejeune. Ionization and acceleration processes in a small, variable channel width, permanent-magnet Hall thruster. *J. Phys. D: Appl. Phys.*, 45:185203, 2012.
[19]A. Lejeune, G. Bourgeois, and S. Mazouffre. Kr II and Xe II axial velocity distribution functions in a cross-field ion source. *Phys. Plasmas*, 19:073501, 2012.
[20]R. Joussot, L. Grimaud, and S. Mazouffre. Physics of a disk-shaped heated LaB_6 cathode for Hall thrusters. In *Proceedings of the 5th Space Propulsion Conference*, Paper 3124900, Rome, Italy, 2016.
[21]S. Mazouffre, S. Tsikata, and J. Vaudolon. Development and experimental characterization of a wall-less Hall thruster. *J. Appl. Phys.*, 116:243302, 2014.
[22]J. Vaudolon, S. Mazouffre, C. Hénaux, D. Harribey, and A. Rossi. Optimization of a wall-less Hall thruster. *Appl. Phys. Letter*, 107:174103, 2015.
[23]I. G. Mikellides, I. Katz, R. R. Hofer, D. M. Goebel, and K. DeGrys. Magnetic shielding of the channel walls in a Hall plasma accelerator. *Phys. Plasmas*, 18:033501, 2011.
[24]I. G. Mikellides, I. Katz, R. R. Hofer, and D. M. Goebel. Magnetic shielding of walls from the unmagnetized ion beam in a Hall thruster. *Appl. Phys. Lett.*, 102:023509, 2013.
[25]I. G. Mikellides, I. Katz, R. R. Hofer, and D. M. Goebel. Magnetic shielding of a laboratory Hall thruster. I. Theory and validation. *J. Appl. Phys.*, 115:043303, 2014.
[26]R. R. Hofer, D. M. Goebel, I. G. Mikellides, and I. Katz. Magnetic shielding of a laboratory Hall thruster. II. Experiments. *J. Appl. Phys.*, 115:043304, 2014.
[27]S. Mazouffre, J. Vaudolon, G. Largeau, C. Hénaux, A. Rossi, and D. Harribey. Visual evidence of magnetic shielding with the PPS-Flex Hall thruster. *IEEE Trans. Plasma Sci.*, 42:2668–2669, 2014.
[28]I. G. Mikellides, I. Katz, R. R. Hofer, and D. M. Goebel. Magnetic shielding of Hall thrusters at high discharge voltages. *J. Appl. Phys.*, 116:053302, 2014.
[29]L. Grimaud and S. Mazouffrel. Ion behavior in low-power magnetically shielded and unshielded Hall thrusters. *Plasma Sources Sci. Technol.*, 26:055020, 2017.
[30]R. W. Conversano, D. M. Goebel, R. R. Hofer, I G. Mikellides, and R. E. Wirz. Performance analysis of a low-power magnetically shielded hall thruster: Experiments. *J. Propul. Power*, 33:975–983, 2017.
[31]R. W. Conversano, D. M. Goebel, I. G. Mikellides, R. R. Hofer, and R. E. Wirz. Performance analysis of a low-power magnetically shielded hall thruster: Computational modeling. *J. Propul. Power*, 33:992–1001, 2017.
[32]B. Karadag, S. Cho, Y. Oshio, Y. Hamada, I. Funaki, and K. Komurasaki. Preliminary Investigation of an External Discharge Plasma Thruster. In *Proceedings of the 52nd Joint Propulsion Conference*, AIAA paper 2016–4951, Salt Lake City, Utah, 2016.
[33]A. M. Kapulkin, A. D. Grishkevich, and V. F. Prisnyakov. *Outside electric field thruster*. Proceedings of the 45th IAF Congress; Space Technol., Vol. 15. (Pergamon, UK), 1995. pp. 391–394.
[34]V. F. Prisnyakov, A. N. Petrenko, A. M. Kapulkin, I. N. Statsenko, A. I. Kondratiev, and S. N. Kulagin. The review of the works on electrical propulsion thrusters development and investigation carried out at the Dnepropetrovsk State University. In *Proceedings of the 24th International Electric Propulsion Conference*, IEPC paper 95–12, Moscow, Russia, 1995.
[35]V. V. Zhurin, H. R. Kaufmann, and R. S. Robinson. Physics of closed drift thrusters. *Plasma Sources Sci. Technol.*, 8:R1–R20, 1999.
[36]S. Mazouffre, S. Tsikata, and J. Vaudolon. Development and characterization of a wall-less Hall thruster. In *Proceedings of the 50th Joint Propulsion Conference*, AIAA paper 2014–3513, Cleveland, OH, 2014.
[37]S. Mazouffre. Laser-induced fluorescence diagnostics of the cross-field discharge of Hall thrusters. *Plasma Sources Science and Technology*, 22:013001, 2013.
[38]S. Mazouffre. *Laser-induced fluorescence spectroscopy applied to electric thrusters*. STO-AVT-VKI Lecture series 263, Electric propulsion systems. Von Karman Institute, Edited by T. Magin, 2016. pp. 10–1..26.
[39]G. Bourgeois, S. Mazouffre, and N. Sadeghi. Unexpected transverse velocity component of Xe^+ ion near the exit plane of a Hall thruster. *Phys. Plasmas*, 17:113502, 2010.
[40]E. Y. Choueiri. Plasma oscillations in Hall thrusters. *Phys. Plasmas*, 8:1411–1426, 2001.

[41] J. P. Boeuf and L. Garrigues. Low frequency oscillations in a stationary plasma thruster. *J. Appl. Phys.*, 84:3541–3554, 1998.

[42] S. Barral and E. Ahedo. Low-frequency model of breathing oscillations in Hall discharges. *Phys. Rev. E*, 79:046401, 2009.

[43] A. McAndrew. *An Introduction to Digital Image Processing With Matlab*. Course Technology Press, Boston, MA, 2004.

[44] J. Vaudolon, L. Balika, and S. Mazouffre. Photon counting technique applied to time-resolved laser-induced fluorescence measurements on a stabilized discharge. *Rev. Sci. Instrum.*, 84:073512, 2013.

[45] J. Vaudolon and S. Mazouffre. Observation of high-frequency ion instabilities in a cross-field plasma. *Plasma Sources Sci. Technol.*, 24:032003, 2015.

[46] A. L. Fabris, C. Young, and M. A. Cappelli. Time-resolved laser-induced fluorescence measurement of ion and neutral dynamics in a Hall thruster during ionization oscillations. *J. Appl. Phys.*, 118:233301, 2015.

[47] A. Diallo, S. Keller, S. Shi, Y. Raitses, and S. Mazouffre. Time-resolved ion velocity distribution in a cylindrical Hall thruster: Heterodyne-based experiment and modeling. *Rev. SCI. Instrum.*, 86:033506, 2015.

[48] D. Tskhakaya, K. Matyash, R. Schneider, and F. Taccogna. The Particle-In-Cell Method. *Contrib. Plasma Phys.*, 47:563–594, 2007.

[49] K. Matyash, R. Schneider, O. Kalentev, Y. Raitses, and N. J. Fisch. Numerical investigations of a cylindrical Hall thruster. In *Proceedings of the 32nd International Electric Propulsion Conference*, IEPC paper 2011–070, Wiesbaden, Germany, 2011.

[50] K. Matyash, R. Schneider, S. Mazouffre, Y. Raitses, and A. Diallo. 3D simulation of rotating spoke in a Hall thruster. In *Proceedings of the 33rd International Electric Propulsion Conference*, IEPC paper 2013–307, Washington, D.C., 2013.

[51] K. Matyash, R. Schneider, S. Mazouffre, L. Grimaud, and S. Tsikata. Investigation of rotating spoke instabilities in a wall-less Hall thruster. Part II: Simulation. In *Proceedings of the 35rd International Electric Propulsion Conference*, IEPC paper 2017–403, Atlanta, Georgia, 2017.